Plant Soil (2020) 451:459–484
https://doi.org/10.1007/s11104-020-04546-9

REGULAR ARTICLE

Lotus corniculatus-rhizobia symbiosis under Ni, Co and Cr stress on ultramafic soil

Marzena Sujkowska-Rybkowska · Dorota Kasowska · Krzysztof Gediga · Joanna Banasiewicz · Tomasz Stępkowski

Received: 22 December 2019 / Accepted: 22 April 2020 / Published online: 13 May 2020

Abstract

Aims Ultramafic/serpentine soils constitute a stressful environment with many plant growth constrains such as a lack of macronutrients and high levels of potentially toxic metals. We considered the adaptive strategy of *Lotus corniculatus* L.-rhizobia symbiosis to Ni, Co and Cr stress conditions.

Methods L. corniculatus nodulating rhizobia from ultramafic soil were isolated, identified and tested for nitrogen fixation, metal tolerance and plant growth promoting abilities. The structural and immunocytochemical analyses of root nodules were also performed.

Results The isolates effective in nitrogen fixation were identified as *Rhizobium* and *Mesorhizobium* tolerant to Ni, Co, and Cr. Some strains directly promoted root growth of *L. corniculatus* and non-legume *Arabidopsis thaliana* under metal stress. The metal treated nodules showed structural alternations, i.e. enhanced accumulation of phenols and wall thickening with higher cellulose, hemicellulose, pectins, glycoproteins and callose content.

Conclusions Our results revealed that metal tolerant, growth promoting rhizobacteria inhabiting *L. corniculatus* root nodules may improve plant growth in the ultramafic environment. Accumulation of phenols and reorganization of nodule apoplast can counteract harmful effects of Ni, Co and Cr on the symbiosis. These findings imply that *L. corniculatus*-rhizobia symbiosis is an important element of plant adaptation to metal stress occurring on the ultramafic soils.

Keywords Metal stress · *Lotus corniculatus* · Rhizobia · Plant growth promotion · Nodule apoplast · Ultramafic/serpentine soil

Abbreviations

AGP	Arabinogalactan-protein
CAS	Chrome-Azurol S
EXT	Extensin
IAA	Indole-3-acetic acid
LB	Luria Bertani medium
LM	Light microscopy

Responsible Editor: Antony Van der Ent.

Electronic supplementary material The online version of this article (https://doi.org/10.1007/s11104-020-04546-9) contains supplementary material, which is available to authorized users.

M. Sujkowska-Rybkowska (✉)
Department of Botany, Institute of Biology, Warsaw University of Life Sciences-SGGW, Nowoursynowska 159, 02-776 Warsaw, Poland
e-mail: marzena_sujkowska@sggw.pl

D. Kasowska
Department of Botany and Plant Ecology, Wrocław University of Environmental and Life Sciences, Grunwaldzki Square 24 A,, 50-363 Wroclaw, Poland

K. Gediga
Department of Plant Nutrition, Wrocław University of Environmental and Life Sciences, Grunwaldzka 53, 50-357 Wroclaw, Poland

J. Banasiewicz · T. Stępkowski
Department of Biochemistry and Microbiology, Institute of Biology, Warsaw University of Life Sciences-SGGW, Nowoursynowska 159, 02-776 Warsaw, Poland

OD	optical density
PCR	Polymerase Chain Reaction
PGP	Plant Growth Promotion
PGPB	Plant Growth Promoting Bacteria
PHB	Poly-3-hydroxybutyrate
PSI	Phosphate Solubilization Index
RT	Room temperature
SP	sample point
TEM	Transmission electron microscopy
TF	Translocation factor

Introduction

Ultramafic soils originate from weathered ultramafic rocks such as peridotite and/or serpentinite. These kinds of rocks have similar chemical composition but they differ in their mineral content. Peridotite consists mostly of olivine and pyroxene, whereas serpentinite, formed from peridotite as a result of low-temperature hydratation, is composed mostly of serpentine group minerals (Coleman 1971; Evans et al. 2013). This various mineralogy of the parent rocks is responsible for differentiation of certain ultramafic soil features such as their morphology and mobility of some elements (Alexander 2004; Kierczak et al. 2016). Despite the differences in their origin, ultramafic soils show specific, common physical and chemical features. As habitats for plant life, these soils offer a combination of multiple limitations known as the "serpentine syndrome". Among them, chemical properties such as low availability of calcium in relation to magnesium, deficiency of essential macronutrients (N, P and K) and high levels of potentially toxic metals, mostly Ni, Cr and Co, are especially stressful for plants and most markedly affect the serpentine flora (Brady et al. 2005; Kazakou et al. 2008). These typical of serpentine substrates metals are microelements metabolically important and essential for plant development but toxic when present at excessive concentrations. For instance, Ni is required for urea metabolism (Gerendás et al. 1999), but at elevated levels (> 10 mg kg^{-1}) it causes growth inhibition, chlorosis, necrosis and wilting in non-tolerant plants by impairing a large variety of physiological processes or conditions (e.g., photosynthesis, respiration, water relations, chlorophyll and protein content, metal homeostasis as well as activity of H+-ATPase, and nitrate and glutathione reductase) (Ahmad and Ashraf 2011; Yusuf et al. 2011; Bhalerao et al. 2015).

The ultramafic soils with their unusual chemical composition often support distinctive floras and unique plant communities, which have been of interest to many researchers (e.g. Brooks 1987; Kruckeberg 2002; Proctor 2003; Reeves et al. 2007). In dry grasslands on ultramafic soils in Poland, representatives of *Fabaceae* (legumes) are abundant and frequent floristic components both on natural ultramafic outcrops (Żołnierz 2007) and on ultramafic mine soils (Kasowska and Koszelnik-Leszek 2014). Their ability to grow in metal polluted and low-fertile environments has been explained by their capacity to form symbiotic interactions with nitrogen-fixing rhizobia and, in majority of these species, with arbuscular mycorrhizal fungi (Pajuelo et al. 2011; Hao et al. 2014; Smith and Read 1997). Rhizobia housed in root nodules provide the plant with reduced nitrogen in exchange for photosynthates (Vincent 1970). Despite comprehensive research on deleterious effects of metals on the rhizobia, nodulation and nitrogen fixation ability of non-metal tolerant legumes (Chaudri et al. 1993; Zahran 1999; Gruber and Galloway 2008; Giller et al. 2009; Franzini et al. 2010; Lafuente et al. 2010), little is known about the effect of metals on the nodule structure and functioning (Ibekwe et al. 1995; Wani and Khan 2013; Sujkowska-Rybkowska and Ważny 2018). Nodules represent a unique environmental niche for symbiont accommodation and proliferation, by providing microsites in metal-contaminated soils where the toxic influence of ions may be limited. On the other hand, in metal polluted soils nodules are the main sites of metal accumulation (Gopalakrishnan et al. 2015). To understand the possible adaptive mechanisms of legume–rhizobia symbiosis to metal stress conditions it is necessary to determine cellular organization of nodules. The most important alteration under toxic metals observed in nodules is thickening of their cell walls that may prevent symbiosis impairment by metal stress (Sujkowska-Rybkowska and Borucki 2012, 2015; Sujkowska-Rybkowska and Ważny 2018). Plant cell wall is the first barrier against toxic metals and wall thickening is one of metal exclusion strategy in plants (Le Gall et al. 2015). The cell wall structure comprising cellulose microfibrils and non-cellulosic neutral polysaccharides embedded in pectin matrix with proteins and phenolic compounds, confers metal binding ability (Probst et al. 2009; Krzesłowska 2011). Excess accumulation of toxic metals in the wall often leads to its stiffening and thickening (Probst et al. 2009; Krzesłowska 2011).

Lotus-rhizobia symbiosis is highly specific and *Lotus* species are nodulated by *Mesorhizobium loti, Bradyrhizobium* sp., *Rhizobium* sp. and *Ensifer* sp. with different levels of effectiveness (see review Lorite et al. 2018). This effectiveness depends on the habitat conditions and little is known about natural rhizobia population associated with native legumes growing on ultramafic soils (Mengoni et al. 2010). Some rhizobia may improve plant growth (plant growth promoting bacteria – PGPB) on contaminated soils through synthesis of phytohormones, siderophores, phosphate solubilization, and reduction of toxic effects of metals (Wani et al. 2007; Karthik et al. 2017). Phytohormones (e.g. auxins) produced by rhizosphere microbe enhance plant growth by directly promoting cell division, cell elongation, root initiation, and/or altering expression of specific genes (Taghavi et al. 2009; Davies 2010). Phosphate solubilizing bacteria can strongly increase phosphorus uptake by plants (Rodríguez and Fraga 1999), and siderophore increases the amount of bioavailable iron at metal contaminated sites (Ma et al. 2011). The siderophore can also form stable complexes with metals, thus decreasing their mobility (Neubauer et al. 2000). Apart from the ability to establish nitrogen-fixing symbiosis, many rhizobia are known to form growth promoting associations with non-legumes, such as maize, rice (Gutiérrez-Zamora and Martínez-Romero 2001; Ladha and Reddy,2003) and *Arabidopsis* (Zhao et al. 2017). One of the main challenges in PGPB research is to understand how the taxonomic diversity of PGPB is related to their efficiency in plant growth promotion under different stresses.

Lotus corniculatus L. (bird's foot trefoil) is one of the most scientifically and ecologically important *Lotus* species (Escaray et al. 2012). This legume is a pioneer plant colonizing marginal and polluted soils and it is the most commonly used *Lotus* species for restoration of contaminated sites (de los Santos et al. 2001; Escaray et al. 2012). It can grow on alkaline or acidic soils and shows high tolerance to aluminum, manganese and salinity (Blumenthal and McGraw 1999). It naturally occurs on different metal-rich soils including ultramafic ones (Banuelos et al. 1992; Hao et al. 2014; Kasowska and Koszelnik-Leszek 2014; Mohamad et al. 2016; Fagorzi et al. 2018), which indicates its high adaptability. However, the knowledge about metal tolerance ability of ultramafic legumes and their associated rhizobia, including their diversity, metal-tolerance, plant growth promoting abilities and symbiotic relations is limited (Abou-Shanab et al. 2007; Pal et al. 2007; Rajkumar et al. 2009; Mengoni et al. 2010; Lorite et al. 2018). These natural metal-tolerant, nitrogen fixing, growth promoting rhizobia are of a great importance for their potential use in agriculture and phytoremediation of metal contaminated areas (Hao et al. 2014).

Considering the above, in the present study we analysed some mechanisms of *L. corniculatus*-rhizobia symbiosis on the ultramafic soil and investigated the plant and rhizobial adaptations to these soil constrains. Our aim was to work out the answers to the following research questions: (i) What is a taxonomic position of the nodulated rhizobia and do they tolerate Ni, Cr and Co? (ii) Are the strains effective in nitrogen fixation and do they exhibit plant growth promoting abilities in the presence of toxic metals? (iii) Does the nodule structure change under metal stress? and (iv) Are the observed alterations a manifestation of adaptation strategy to the presence of toxic metals?

Materials and methods

Study area and samples collection

Ultramafic rocks and their soils in Poland occur as a few outcrops only within the Sudetes (Lower Silesia region, SW Poland). They form here a few small bodies and larger massifs with one of the largest – the Szklary Massive. The Szklary Massive outcrop is located within the Fore Sudetic Block and is composed of partially serpentinized peridotites cut by subordinate granitoids and lamprophyre veins (Kierczak et al. 2007). Geographically, the Szklary Massive lays in the Sudetic Foothills within the Niemczańsko-Strzelińskie Hills (Supplement, Fig. S1).

The partially serpentinized peridotite from the Szklary Massif consists mainly of serpentine, olivine, and amphiboles. It contains relatively high amounts of Ni (up to 2341 mg kg^{-1}), Cr (up to 2915 mg kg^{-1}) and Co (up to 164 mg kg^{-1}). The most important source of Ni are there olivine and serpentine, while Cr and Co are mostly bounded in spinel group minerals The soil type formed on this bedrock was classified as Eutric Leptosol (Humic, Magnesic; Kierczak et al. 2016). On the area of the Szklary Massive, exploitation of nickel ores took place from the end of 19th century. The excavation has been done by underground techniques initially and then by surface mining. Mining and Smelting Plant in

Szklary operated until 1983, and after the mine has been closed their area was reclaimed and forested in the overwhelming. Some slopes of excavations and the mine pit terrain were revegetated in the spontaneous succession process. Their flora and its ecological characteristic were described by Kasowska (2005) and Kasowska and Koszelnik-Leszek (2014).

L. corniculatus plants and ultramafic soil were taken in June 2016 from the mine pit surface (N 50°38'81.4"-50°38'83.2"; E 16°50'21.2"-16°50'20.9") at sites where this species dominated in the plant cover from three sample points (SP). At least three specimens were collected from each SP for obtaining a representative sample. These samples consisted of both the plants, being at the flowering phase, and the soil bulk, containing the roots and the soil of the rooting zone (10-20 cm depth). The soil bulks were moisturized with tap water and the whole samples were packed into plastic bags and taken to a laboratory as soon as possible to preserve rhizobia vitality. Seeds of *L. corniculatus* were further taken in the same sample points in August 2016.

Content of Ni, Cr and Co in ultramafic soil and plant parts

Soil samples, received from the soil bulks, were air-dried and sieved through a 2-mm sieve. The total concentration of Ni, Cr and Co was determined after soil digestion in aqua regia according to ISO 11466.3. Soil samples weighed to 0.250 g were placed in a 250 ml Pyrex Erlenmeyer flasks. The pre-digestion step was done at room temperature (RT) for 24 h with a mixture of 12 M HCl and 17 M HNO_3 in the 3:1 (v/v) ratio. The obtained suspensions were digested on a hot plate at 130 °C for 15 min. Then, they were cooled until RT, filtered through an ashless Whatman 41 filter and, finally, diluted to 25 ml with 0.17 M HNO_3.

The geochemically reactive forms of the studied elements were analyzed after extraction in 0.43 M HNO_3 (Groenenberg et al. 2017). The extraction solution was prepared by dilution of 30 mL concentrated HNO_3 (65%, Merck, analytical grade) in 1000 mL ultrapure water. The samples were shaken during 2h with soil: solution ratio 1:10 (weight/volume). The concentrations of both total and reactive forms of metals were determined by atomic absorption spectrometry with a Varian SpectrAA 220FS apparatus. Samples of birdsfoot trefoil shoots and roots, separated from the soil bulks, were thoroughly washed with tap and distilled water, and dried at 40°C. Ground plant material was oven ashed at 475°C overnight. Concentration of metals, after ash dissolution in 6M HCl (Sillanpää 1982), were determined with a Varian SpectrAA 220FS AAS apparatus. The samples from each SP were analysed separately and all analysis and measurements were done in two analytical replicates. To determine L. corniculatus ability to transferring metals from roots to aboveground parts the translocation factor (TF) was evaluated as a ratio of the metal content (mg kg^{-1}) in the shoots to this metal content (mg kg^{-1}) in the roots.

Strain isolation and molecular identification

Because of the very small amount of nodules occurred at the ultramafic *L. corniculatus* roots, the plant specimens collected at all SPs were pooled to obtain enough material for all microbiological tests. For rhizobia isolation, about twenty nodules, at least two effective ones per ultramafic plant, were used. Rhizobia strains were isolated according to Vincent (1970) method and grown on YEM medium. The nodulation ability of isolated strains were performed in the authentication test on serpentine bird's foot plants. The seeds of *L. corniculatus* were scarified with 96% sulfuric acid (H_2SO_4) for 6 minutes and washed in sterile deionized water five times and after germination for 3 days on Petri dishes containing 1% water agar were transferred to pots (5 seedlings per pot) filled with sterile ultramafic soil and singly inoculated. Soil was sterilized for 3 days at 100 °C for 1h each day and then allowed to cool for 72 h (Ogar et al. 2015). The effectiveness of soil sterilization was confirmed by the lack of nodules on non-inoculated plants and their rapid death.

Thirty-three isolates formed nodules on bird's foot roots during the authentication test and were initially characterized by rep-PCR (BOXA1R) analysis. The primer BOXA1R (5' CTACGGCAAGGCGA CGCTGACG 3' (Versalovic et al. 1994; Koeuth et al. 1995) was used to generate BOX-PCR profiles of isolates. Reactions were denatured at 95°C for 2 min, subjected to 35 cycles of 95°C for 30 s, 53°C for 30 s and 72°C for 8 min. A final extension at 72°C for 7 min was added. PCR mixtures were set up as per manufacturers protocol with DreamTaqTM DNA Polymerase (Thermo Fisher Scientific, USA). BOX-PCR profiles were visualized by separation on 1% agarose gel electrophoresis using a The PowerPac™ Universal power supply (Bio-Rad Laboratories, USA), using Tris–

acetate–EDTA buffer. A molecular weight marker (GeneRuler 1 kb DNA Ladder, Thermo Fisher Scientific, USA) was included in all gels. Gels run at 26°C at 100 V constant voltage, until the TriTrack DNA Loading Dye (6X) (Thermo Fisher Scientific, USA) reached the bottom of the gel. The gels were stained with SimplySafe™ (EURX, Poland) (Supplement, Fig. S2). Twenty three strains representing different types of BOX were selected for further analysis with two housekeeping gene markers (*glnII* and *dnaK*) to assess the level of diversity of the selected isolates. Primers used for PCR amplification are listed in Table 1.

PCR amplification reactions were performed following the procedures described elsewhere (Stępkowski et al. 2005; Beukes et al. 2016). The reaction mixture was first denatured at 95°C for 2 min and then subjected to 35 cycles of denaturation at 95°C for 30 s, annealing at 60°C (*glnII)* or 55°C (*dnaK*) for 30 s, elongated at 72°C for 1.5 min and a final elongation step was conducted at 72°C for 7 min. In all PCR reactions DreamTaq^{TM} DNA Polymerase (Thermo Fisher Scientific, USA) was used. PCR products were purified with an ExtractMe DNA-gel-out kit (BLIRT, Poland) and sequenced on an ABI3100 Automated Capillary DNA sequencer (Applied Biosystems, USA). Sequence chromatograms were visualized and manually edited using BioEdit and the generated sequences subjected to BLASTn searches (Altschul et al. 1990; Benson et al. 2005).

Estimation of bacterial metals tolerance

All strains were checked for Ni, Co and Cr tolerance on SLP (Jiang et al. 2008) agar plates (not shown). 1mM stock solutions of metals salts sterilized by filtration (0.20 μm) was added to sterile agar SLP medium as follow: Ni 0.2mM, 2mM and 5mM as $NiSO_4$; Co 2mM, 5mM and 10mM as $CoCl_2$; and Cr 2mM, 5mM and 10mM as K_2CrO_4. Selection of the chemical compounds and concentrations used in the experiment was made on the basis of previous studies described in the literature (Rooney et al. 2007; Li et al. 2009; Wani and Khan 2013) and these metal doses were comparable to the total and/or the reactive forms in the examined ultramafic soil from which the bacteria strains were isolated. Additionally, for strains with the highest metal tolerance, the analysis of bacterial growth in liquid SLP medium supplemented with increasing concentrations of metals was performed. The strains were grown in liquid medium for 72 h at 28°C and 100 μl of 10^8 cell/ml bacterial culture were deposited onto SLP agar plates and incubated at 28°C for 24–72 h. The test in liquid SLP medium was carried out with the same metals concentrations and bacterial growth has been measured at based on the absorbance at 600 nm using a Biospectrometer (Eppendorf). Three replicates were made for each bacterial strain and each test was repeated three times.

Table 1 Oligonucleotides used for PCR amplification

Primer	Gene	Sequence (5' to 3')	References
TSdnaK4	*dnaK*	GGC AAG GAG CCG CAY AAG G	Stępkowski et al. (2007)
TSdnaK2		GTA CAT GGC CTC GCC GAG CTT CA	Stępkowski et al. (2003)
TSglnIIf	*glnII*	AAG CTC GAG TAC ATC TGG CTC GAY GG	Stępkowski et al. (2005)
TSglnIIr		SGA GCC GTT CCA GTC GGT RTC G	Stępkowski et al. (2005)

Determination of Plant Growth Promotion (PGP) traits

All isolated strains were checked for indole acetic acid (IAA) biosynthesis, siderophore production and phosphate solubilization abilities. In the case of nitrogenase activity four strains (L9, L19, L42, L50), most effective in nodulation in the authentication test, were examined for the efficiency in nitrogen fixation. Each test was repeated twice.

IAA estimation was determined in Luria Bertani medium (LB) supplemented with 0.2% tryptophan and/or metals, Ni (0mM, 0.2mM, and 2mM, as $NiSO_4$,), Co (0mM, 2mM, and 5mM as $CoCl_2$) and Cr (0mM, 2mM, and 5mM as K_2CrO_4) and bacterial isolates. After 24h of growth in 28^0C, the cultures were centrifuged and two milliliters of supernatant of the bacteria culture (10^8 cell/ml bacterial culture) was mixed with 4mL of the Salkowski reagent and after 1h of incubation at 28^0C the absorbance at 530 nm was measured using Biospectrometer (Eppendorf) (Star et al. 2012). The concentration of IAA was calculated using a calibration curve of pure IAA as a standard (Sigma-Aldrich).

Siderophore production was detect using chrome-azurol S (CAS) agar medium (Alexander and Zuberer 1991). Bacterial cultures were grown for 24h in 28^0C in liquid SLP medium without metals or supplemented with metals similar as for metal tolerance tests and then

20μl of each cultures (10^8 cell/ml bacterial culture) were spotted on CAS agar plates and grow at 28^0C for week. The orange haloes around colonies indicates production of siderophores.

Phosphate solubilization ability of bacterial strains was carried out on Pikovskaya (PVK) agar medium (Pikovskaya 1948; Zaidi et al. 2006). The plates were inoculated with 20μl of bacteria culture (10^8 cell/ml) growing in SLP medium with or without metals in doses similar as for metal tolerance tests. After one week of incubation at 28^0C plates were checked for haloes presence. Solubilization potency was measured based on Phosphate Solubilization Index (PSI) as Total diameter of halo zone/Colony diameter (Morales et al. 2011).

Nitrogen fixation capacity was quantified indirectly by acetylene reduction assay (Hardy et al. 1968). After three months of growth in laboratory conditions cut nodules were quickly placed in 5ml glass bottles filled with 10% acetylene, incubated for 1h at 28^0C and ethylene content was measured using a gas chromatograph with a mass spectrometer (ATI Unicam). Nitrogenase activity was expressed in C_2H_4 nanomoles per hour for 1 gram of fresh weight of nodules. The measurement was performed in three technical repetitions.

Roots growth promotion by selected rhizobia

Roots growth promotion ability of most PGP active *Rhizobium* (L9) and *Mesorhizobium* (L42) strains were checked for host birdsfoot trefoil and *Arabidopsis thaliana* L. (*Col*-0) plants. Seeds of ultramafic *L. corniculatus* were prepared as described above. *A. thaliana* seeds were surface sterilized with 0.1% sodium hypochlorite for 5min and washed 20 minutes with distilled water. Subsequently, the both types of seeds were put on vertical placed plates with Gamborg medium (with 1% Bacto Agar) and left to grow for 5 days in constant conditions (16h photoperiod, 22^0C temperature and photon flux density of 170 $\mu mol \cdot m^{-2} \cdot s^{-1}$). Next the seedlings were transferred to fresh Gamborg vertical placed plates (6 plants per plate) supplemented with metals (0; Ni 0.2mM; Co and Cr 0.5mM; doses based on Aka and Babalola 2017) and were or not inoculated with 100μl of freshly prepared L42 or L9 bacterial cultures (optical density of 0.2 at 600 nm). Growth of seedlings was assessed by measuring length of primary root and lateral roots formation after 8 days of growth. Each plate was in triplicate.

Microscopic analysis of nodules

Ultramafic *L. corniculatus* seeds were used to obtain control plants, which were grown for three months in laboratory conditions (14h photoperiod, photon flux density of 300 $\mu mol/m^2/s$, 22°C/17°C day/night regime, 70% relative humidity) in pots filled with sterile keramzyt and inoculated with consortium of isolated rhizobia (L9 and L42) and watered once a week with nitrogen-free Fahreus medium (Vincent 1970).

For microscopic analysis, ten effective nodules, both from the ultramafic soil and the control plants, were used. A part of nodule hand sections were stained with dimethylglyoxime for Ni localization (Seregin and Kozhevnikova 2011) or 1% (v/v) calcofluor white to visualize cellulose under UV (Olympus-Provis, Japan). For (ultra)structural studies collected nodules were fixed in Karnovsky medium for 2h in RT, washed with 0.1M cacodylate buffer, and subjected to a routine preparation procedure for epoxy resin, described previously (Sujkowska-Rybkowska and Borucki 2012). The semi-thin sections stained with 1% toluidine blue or 1% alcoholic solution of safranin-O (Broda 1971) for phenolic inclusions demonstration were analysed under light microscopy (Olympus-Provis, Japan). Ultrathin sections collected on formvar-coated grids, short stained with uranyl acetate and lead citrate were examined under a transmission electron microscope (Morgagni). Digital images were saved as jpg files and if necessary were adjusted using Photoshop CS 8.0 (Adobe Systems, USA) software by non-destructive tools (levels and/or contrast) throughout the whole area of an image. The figures were prepared using the Corel DRAW 11 software (Corel Corporation, Canada).

Immunolocalization of cell wall components in nodules

Ten nodules from five plants, both from the ultramafic soil and the control were sampled, then fixed in 4% paraformaldehyde in MSB buffer for 2h in RT and subjected to a routine procedure for BMM resin embedding, described previously (Sujkowska-Rybkowska and Borucki 2015). Semi-thin sections of nodules embedded in BMM resin were transferred to silane-prep slides (Sigma-Aldrich). Some sections were stained with 1% toluidine blue for light microscopy and other were blocked with 3% bovine serum albumin (BSA) (Sigma-Aldrich) in 0.01M PBS buffer for 1h at RT. After three washing with 0.01M PBS, several primary rat

monoclonal antibodies: LM19 (anti-unesterified homogalacturonan HG); LM20 (anti-partially methyl-esterified HG); LM25 (anti-xyloglucan); LM1, JIM11 and JIM12 (anti-extensin EXT); LM2 and JIM13 (anti-arabinogalactan-proteins AGP)(Plant Probes) diluted 1:3 were used, and anti-β-1,3-glucan (anti-callose) mouse antibody (Biosupplies) diluted 1: 40 in PBS containing 0.5% (w/v) BSA was applied overnight at RT. The control consisted of nodules sections non-treated with primary antibody. Following rinsing with PBS the sections were incubated for 1,5 h at RT in PBS containing 0.5% (w/v) BSA and FITC goat anti-rat IgG antibody (Sigma-Aldrich) or Alexa Fluor 488 goat anti-mouse antibody (Invitrogen) diluted 1: 200. After washing with PBS the sections were closed in a drop of PBS and observed under fluorescent microscopy with used of triple DFTR filter (Olympus-Provis, Japan). The obtained digital images were processed as described above. Labeling for each antibody was carried out twice on three different nodules.

Data analysis

Analysis of significant differences among means of the metal contents in *L. corniculatus* organs was performed using the Student's dependent *t*-test. The two-way ANOVA and the post-hoc Tukey HSD test were used for analysis of significant differences among means in the trial of bacterial strains tolerance to metals. In the case of nitrogenase activity, nodule number, root length and number of lateral roots the one-way ANOVA and the post-hoc Tukey HSD test were performed. All analyses have been carried out at the level p=0.05 with Statistica software version 13 (TIBCO Software Inc. 2017).

Results

Ni, Cr and Co content in ultramafic soil

Table 2 shows the content of total and geochemically reactive Ni, Cr and C. Both forms of nickel occurred in significantly higher amounts than other metals, and generally the levels of all elements significantly varied at individual sampling points. Total content of all metals was the highest at SP1 and the lowest at SP3, and total content of Cr and Co was more diverse than that of Ni. The reactive content (0.43 M HNO_3^- extractable forms) can be considered potentially available for uptake by biota. The share of reactive Ni in its total pool was about 50% in all samples and was generally the highest among all metals. The content of reactive Cr and its share in the total pool was the lowest. The reactive Co level was higher than that of Cr but its share in the total pool varied greatly between the samples.

Ni, Cr and Co content in *L. corniculatus* organs and metal translocation

Table 3 presents mean content of Ni, Cr and Co in shoots and roots of *L. corniculatus* from the ultramafic soil. Nickel was present at significantly higher levels than Cr and Co both in the roots and shoots, and the content of Ni in the roots exceeded 100 mg kg^{-1}. Accumulation of all metals was significantly higher in the roots than in the shoots but in the case of Co the difference was not statistically significant (*t*-test, $p \geq 0.05$). Translocation factor (TF) indicates a plant species tolerance strategy to high levels of metals. In *L. corniculatus*, its value fell below 1 for all studied elements.

Comparative analysis of rhizobial sequences

GlnII gene was amplified for 18 strains and *dnaK* for 21 strains. Preliminary results of sequence analysis of *dnaK* and *glnII* genes and alignment with databases deposited in NCBI GenBank revealed that the isolates represented the genera *Rhizobium* and *Mesorhizobium* (see Table 4). Blast searches of partial *glnII* and *dnaK* sequences revealed that the 18 isolates belonged to either *Rhizobium* or *Mesorhizobium* species (Table 4). Strains L9, L10, L11, L14, L16, L19, and L20 exhibited the highest similarity (95.8% -100%) to *Rhizobium leguminosarum* or a closely related species. Contrary to that, strains L6, L17, L25, L26, L27, L28, and L37 represented a new lineage within the genus *Rhizobium*, showing <90% similarity to other *Rhizobium* species, for instance, to *R. lusitanum* strain P1-7 (not shown). For *dnaK* sequences, these similarity values were somewhat higher; for instance, strain L6 showed 92.95% similarity to *R. giardinii* bv. *giardinii* type strain H152, and 92.2% to *R. rhizosphere* MH17, respectively. Table 4 contains the highest similarity values (92.1%-93.3%) of these strains with respect to several unclassified *Rhizobium* strains. Strains L31, L35, L42, and L50 belonged to *Mesorhizobium septentrionale* (98.6%-100%), while

Table 2 Content of the total and the geochemically reactive Ni, Cr and Co ($mg \cdot kg^{-1}$) in the ultramafic soil samples from Szklary nickel ore mine; SD- standard deviation

	Ni		Cr		Co	
Sample point	total	reactive	total	reactive	total	reactive
SP1	1705.3	844.0	355.0	10.5	228.0	14.7
SP2	1513.1	803.0	68.0	7.7	79.7	18.6
SP3	1269.1	666.0	43.4	7.6	20.4	16.3
Mean±SD	1495.8±178.5	771.0±76.1	155.5±141.4	8.6±1.3	109.4±87.3	16.5±1.6

strains L32 and L36 were most similar to *M. jarvisii* ATCC 33669 (97% similarity). The *Rhizobium* and *Mesorhizobium* strains were hosted by different nodules on the same plant.

Bacterial tolerance to metals

The experiment on solid SLP medium demonstrated the ability of all tested rhizobia to grow in the presence of low doses of Ni (data not shown). The isolates *Rhizobium* (L9, L19) and *Mesorhizobium* (L42, L50) were most effectively growing on Ni-enriched plates and also in the presence of Co and Cr. These strains were further analyzed in liquid medium, where the influence of metals on the bacterial growth was estimated by measuring optical density (OD) at 600 nm (Fig. 1).

In Fig. 1a it can be observed significant higher metal tolerance of *Rhizobium* strains (L9, L19) than *Mesorhizobium* ones (L42, L50) to Ni at its lowest dose (0.2mM). With the intermediate Ni doses (2.0 and 5.0mM) there were no statistically significant difference among *Rhizobium* (L9, L19) and *Mesorhizobium* (L42, L50) strains. The tolerance of *Rhizobium* strains (L9, L19) to Co were significantly higher compare to *Mesorhizobium* ones (L42, L50) from low to highest Co doses (Fig. 1b). The observed significant increase in *Rhizobium* (L9, L19) growth at the intermediate Co doses compare to the lowest Co level (0.2mM) would suggest the higher tolerance of these strains to Co than in the case of *Mesorhizobium* ones. However, the general dose response of *Mesorhizobium* (L42, L50) strains to Co were similar to *Rhizobium* ones but the effects were not statistically significant. In the case of Cr, statistically significant decrease of all strains growth, both *Rhizobium* and *Mesorhizobium,* occurred compare to control. However, like after applying Co, *Rhizobium* (L9, L19) strains were more tolerant but the differences in relation to *Mesorhizobium* were not statistically significant (Fig. 1c). In both genera, the highest concentrations of Co and Cr negatively affected bacterial growth while medium doses of these metals stimulated this process after a significant growth drop at the lowest Co and Cr levels (Fig. 1b and c).

Table 3 Content of Ni, Cr and Co ($mg\ kg^{-1}$) in shoots and roots of *L. corniculatus* from the ultramafic soil given as mean ± standard deviation with metal translocation factors (TF); *t*-test probability level (p) for comparison of means of shoots and roots, significant differences with $p \leq 0.05$

	Ni	Cr	Co
Shoots	59.5±19.4	5.4±1.3	2.4±0.8
Roots	167.1±24.6	20.5±3.2	8.5±2.8
p	0.01	0.03	0.06
TF	0.36	0.26	0.28

Bacterial PGP features

In control (non-metal conditions) all strains were capable of solubilizing phosphate, fourteen strains produced siderophore and six synthesized IAA (Table 5). Four metal-tolerant strains of *Rhizobium* (L9 and L19) and *Mesorhizobium* (L42 and L50) exhibited higher PGP abilities in the presence of Ni, Co and Cr (Table 5). Under metal stress, both genera increased their production of IAA. A maximum amount of IAA (9.6μg/ml) was produced by L9 strain growing in LB broth supplemented with 5mM Cr. These strains intensified also siderophore production to make iron more bioavailable under presence of any dose of Ni. Application of 2mM Co and Cr curbed siderophore synthesis in L9 and L42 strains. Furthermore, all strains were capable of phosphate solubilization on agar medium in presence of nickel. Ni increased phosphorus solubilization potential

Table 4 Identification based on *glnII* and *dnaK* genes sequences of the rhizobia isolated from *L. corniculatus* nodules collected from ultramafic soil

Strains ID	Name of bacteria	Best match sequence/ accession number	Similarity (%)
glnII			
L6	*Rhizobium* sp.	*Rhizobium* sp. CCBAU 01209	93.3%
L9	*Rhizobium leguminosarum*	*Rhizobium leguminosarum* bv. *viciae* UPM791	99%
L10	*Rhizobium leguminosarum*	*Rhizobium leguminosarum* RMCC TP0512	95.8%
L11	*Rhizobium leguminosarum*	*Rhizobium leguminosarum* EU155089.1	98.4%
L14	*Rhizobium leguminosarum*	*Rhizobium leguminosarum* bv. *viciae* KJ923061.1	99.8%
L16	*Rhizobium leguminosarum*	*Rhizobium leguminosarum* CP025012.1	94.8%
L17	*Rhizobium* sp.	*Rhizobium* sp. EU513321.1	93.3%
L19	*Rhizobium leguminosarum*	*Rhizobium leguminosarum* bv. *viciae* CP025509.1	100%
L20	*Rhizobium* sp.	*Rhizobium* sp. EU513321.1	92.5%
L25	*Rhizobium* sp.	*Rhizobium* sp. EU513321.1	92.2%
L26	*Rhizobium* sp.	*Rhizobium* sp. EU513321.1	93.3%
L27	*Rhizobium* sp.	*Rhizobium* sp. EU513321.1	92.2%
L28	*Rhizobium* sp.	*Rhizobium* sp. EU513321.1	92.4%
L29	*Rhizobium* sp.	*Rhizobium* sp. EU513321.1	92.4%
L37	*Rhizobium* sp.	*Rhizobium* sp. EU513321.1	93.1%
L36	*Mesorhizobium* sp.	*Mesorhizobium* sp. KJ556475.1	97.4%
L42	*Mesorhizobium septentrionale*	*Mesorhizobium septentrionale* FM164387.1	98.6%
L50	*Mesorhizobium septentrionale*	*Mesorhizobium septentrionale* EU513300.1	100%
dnaK			
L6	*Rhizobium* sp.	*Rhizobium* sp. CP032509.1	92.4%
L9	*Rhizobium leguminosarum*	*Rhizobium leguminosarum* bv. *viciae* CP025509.1	100%
L10	*Rhizobium* sp.	*Rhizobium* sp. CP013643.1	96.5%
L11	*Rhizobium leguminosarum*	*Rhizobium leguminosarum* bv. *viciae* CP025509.1	100%
L14	*Rhizobium leguminosarum*	*Rhizobium leguminosarum* bv. *viciae*	99.8%
L15	*Rhizobium leguminosarum*	AM236080.1	100%
L16	*Rhizobium leguminosarum*	*Rhizobium leguminosarum* bv. *viciae* CP025509.1	94.8%
L17	*Rhizobium* sp.	*Rhizobium leguminosarum* CP030760.1	92.1%
L19	*Rhizobium leguminosarum*	*Rhizobium* sp. CP032509.1	100%
L20	*Rhizobium* sp.	*Rhizobium leguminosarum* bv. *viciae* CP025509.1	98.1%
L25	*Rhizobium* sp.	*Rhizobium leguminosarum* CP030760.1	89.7%
L26	*Rhizobium* sp.	*Rhizobium* sp. CP013511.1	89.9%
L27	*Rhizobium* sp.	*Rhizobium* sp. CP020947.1	89.9%
L29	*Rhizobium* sp.	*Rhizobium* sp. CP020947.1	89.9%
L37	*Rhizobium* sp.	*Rhizobium* sp. CP032509.1	90.4%
L31	*Mesorhizobium septentrionale*	*Rhizobium* sp. CP032509.1	98.6%
L32	*Mesorhizobium* sp.	*Mesorhizobium septentrionale* FM164387.1	97.2%
L35	*Mesorhizobium septentrionale*	*Mesorhizobium* sp. CP034453.1	98.6%
L36	*Mesorhizobium* sp.	*Mesorhizobium septentrionale* FM164387.1	97.2%
L42	*Mesorhizobium septentrionale*	*Mesorhizobium* sp. CP034453.1	98.6%
L50	*Mesorhizobium septentrionale*	*Mesorhizobium septentrionale* FM164387.1	98.6%
		Mesorhizobium septentrionale FM164387.1	

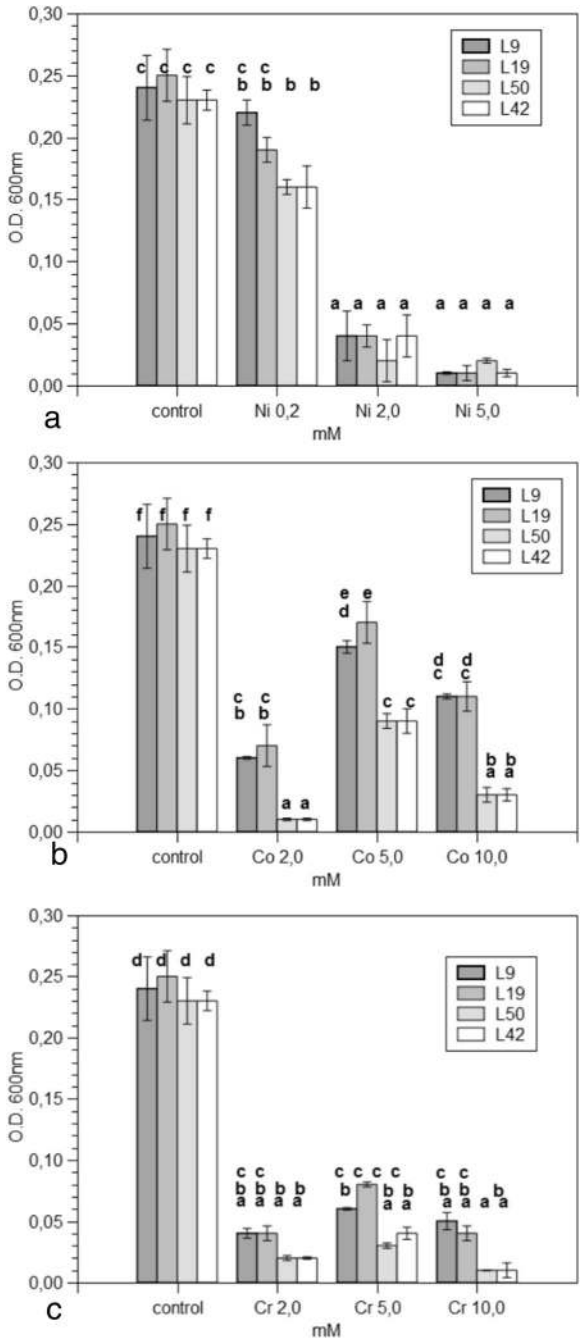

Fig. 1 a-c. Optical density of *Rhizobium* (L9 and L19) and *Mesorhizobium* (L50 and L42) isolates at different Ni, Co and Cr concentrations after 72h of growth. Values are means ± SD from three independent experiments. The same letters indicate the homogenous groups according to the Tukey HSD test at the level p=0.05

(PSI 5.0) in L9 and L19, and PSI 4.0 for L42 and L50 strains, while the presence of Co and Cr inhibited this ability.

Nitrogenase activity and nodulation

Four strains (L9, L19, L42, L50) most effective in nodulation in the authentication test were examined for their efficiency of nitrogen fixation. *Mesorhizobium* strain L42 was the most efficient of all examined strains, and showed the significantly highest nitrogenase activity and nodulation per plant compare to other strains. *Rhizobium* strains L19 alike L9 was the lowest in nitrogenase activity as well in nodulation (Fig. 2).

Direct root growth promotion and lateral root formation of Arabidopsis thaliana and L. corniculatus colonized by *Rhizobium* and *Mesorhizobium*

Two isolates, *Rhizobium* L9 and *Mesorhizobium* L42 which showed high nitrogen fixation ability, highest PGP traits and Ni tolerance were evaluated for in vivo PGP potential with their original host *L. corniculatus* and non-legume *A. thaliana* (Fig. 3). Root growth and lateral roots formation of *A. thaliana* and *L. corniculatus* were significantly inhibited by metals (Ni 0.2mM, Co and Cr 0.5mM). Inoculation by *Rhizobium* L9 and *Mesorhizobium* L42 alleviated to some extent these negative effects, and in the case of *L. corniculatus*, the statistically significant increase in the number of lateral roots was found for both rhizobia strains. However, it seems that *Rhizobium* L9 was more effective in the root growth promotion and the roots formation under metal stress. The inoculated and unexposed to toxic metals plants had longer the main root and formed more lateral roots compare to control, and these effects were statistically significant for *Rhizobium* L9 with only one exception of the number of roots in *L. corniculatus*. *Mesorhizobium* L42 favored the root growth and the lateral roots formation but the differences between means, in relation to control, were not statistically significant.

Structural analysis of *L. corniculatus* nodules

The ultramafic *L. corniculatus* involved small plants with a thick main root and pink and apparently functional nodules formed on thin lateral roots (Fig. 4a). The nodules were determinate, more-or-less spherical with many striped lenticels on their surface (Fig. 4b). They were active in nitrogen fixation, as indicated by red color (leghemoglobin) of their interior (Fig. 4c). The

Table 5 Plant growth promoting (PGP) activities of isolates

Characteristic	L6	L9	L10	L11	L14	L16	L17	L19	L20	L25	L26	L27	L28	L29	L37	L36	L42	L50
IAA μg/ml +0.2% tryptophan																		
0 mM	-	1.3 ± 0.1	-	-	0.8 ± 0.2	-	-	1.0 ± 0.1	-	-	-	-	-	-	-	0.8 ± 0.2	1.0 ± 0.1	1.0 ± 0.1
Ni 0.2mM	-	5.5 ± 0.2	-	-	0.8 ± 0.1	-	-	5.0 ± 0.7	-	-	-	-	-	-	-	1.0 ± 0.9	4.6 ± 0.1	4.0 ± 0.6
Ni 2 mM	-	2.5 ± 0.1	-	-	0.5 ± 0.1	-	-	2.2 ± 0.4	-	-	-	-	-	-	-	1.1 ± 0.9	2.6 ± 0.5	2.0 ± 0.8
Co 2 mM	-	1.2 ± 0.2	-	-	0.8 ± 0.1	-	-	1.1 ± 0,1	-	-	-	-	-	-	-	1.2 ± 0.1	2.3 ± 0.1	2.1 ± 0.1
Co 5 mM	-	2.5 ± 0.1	-	-	0.5 ± 0.3	-	-	2.3 ± 0.1	-	-	-	-	-	-	-	2.0 ± 0.1	2.4 ±0.1	2.2 ± 0.1
Cr 2 mM	-	7.3 ± 0.2	-	-	2.0 ± 0.2	-	-	7.1 ± 0.2	-	-	-	-	-	-	-	2.1 ± 0.3	6.0 ± 0.2	4.9 ± 0.2
Cr 5 mM	-	9.6 ± 0.6	-	-	1.8 ± 0.1	-	-	9.0 ± 0.1	-	-	-	-	-	-	-	3.2 ± 0.5	8.7± 0.1	7.8 ± 0.1
Siderophores on CAS agar																		
0 mM	+	+++	-	-	+	-	-	++	+	+	+	+	+	+	+	+	+++	+++
Ni 0.2 mM	+	+++	-	-	+	-	-	++	+	+	+	+	+	+	+	+	++	++
Ni 2 mM	-	+++	-	-	-	-	-	++	-	-	-	-	-	-	-	-	++	+
Co 2 mM	-	++	-	-	+	-	-	+	+	+	+	+	+	+	+	+	++	+
Co 5 mM	-	-	-	-	-	-	-	-	-	-	-	-	-	-	-	-	-	-
Cr 2 mM	-	++	-	-	+	-	-	+	-	-	-	-	-	-	-	+	++	+
Cr 5 mM	-	-	-	-	-	-	--	-	-	-	-	-	-	-	-	-	-	-
Phosphate solubilizing potential (PSI*)																		
0 mM	1	2	1	1	1	1	1	2	1	1	1	1	1	1	1	2	2	2
Ni 0.2 mM	1	5	1	1	1	1	1	5	1	1	1	1	1	1	1	2	4	4
Ni 2 mM	1	5	1	-	1	-	-	5	-	-	-	-	-	-	-	2	4	4
Co 2 mM	-	-	-	-	-	-	-	-	-	-	-	-	-	-	-	-	-	-
Co 5 mM	-	-	-	-	-	-	-	-	-	-	-	-	-	-	-	-	-	-
Cr 2 mM	-	-	-	-	-	-	-	-	-	-	-	-	-	-	-	-	-	-
Cr 5 mM	-	-	-	-	-	-	-	-	-	-	-	-	-	-	-	-	-	-

Four level [no production (-), low (+), medium (++) and high (+++) production] were established

*PSI - Phosphate solubilization index

The values are presented as means ± standard deviation

plants and nodules showed no visual toxicity symptoms when they grew on ultramafic soil, and nodules accumulated Ni in nodule cortex tissues (Fig. 4d,e).

Light microscope analyses of ultramafic nodules revealed typical features of determinate nodules, i.e. lack of a meristem and a homogenous population of symbiotic cells in central N_2-fixing zone (Fig. 4f,g). Uninfected cells were devoid of starch granules (Fig. 4g).

The mixture of infected and uninfected cells in the central tissue of the ultramafic and control nodules was surrounded with non-infected cortical cells with vascular bundles (Fig. 5a,m) and numerous dark vacuolar inclusions (phenolic-like substances) were observed in metal-treated nodules (Fig. 5a). The phenolic nature of vacuolar inclusions was confirmed by safranin stain (Fig. 5b, c). The nodule cortex of both nodules contains three to five layers of cortex cells, one or two layers of dark staining nodule endodermis and five to six layers of nodule parenchyma cells (Fig. 5a,m). In ultramafic nodules, parenchyma cells

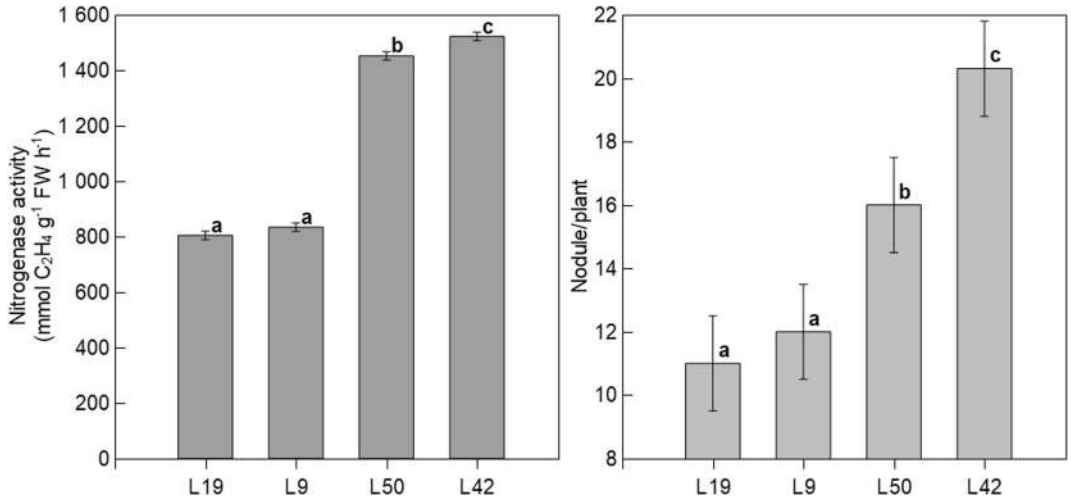

Fig. 2 Nitrogenase activity of nodules and nodules number induced by selected rhizobia, *Rhizobium* (L9 and L19) and *Mesorhizobium* (L50 and L42) on *L. corniculatus* roots growing on sterile ultramafic soil. Error bars represent SD. The same letters indicate the homogenous groups according to the Tukey HSD test at the level p=0.05

were devoid of starch granules in contrast to control ones (Fig. 5a,m,n). Ultrastructural studies confirmed that vacuoles of the cortex tissues were filled with dark phenolic-like substances (Fig. 5d-f). Intercellular spaces of the cortex tissues were large with dark inclusions (Fig. 5g-i). Some dark precipitates were also visible inside the cell wall of the nodule cortex (Fig. 5h), in intercellular spaces (Fig. 5j, k), and vacuoles of uninfected cells (Fig. 5l). In control nodules, phenolic-like substances in nodule cortex tissue occurred sporadically (Fig. 5m-o) and no dark inclusions were present in parenchyma cells or intercellular spaces (Fig. 5n).

The infected cells of ultramafic nodules had one or two large central vacuoles instead of a few small ones observed in control nodules and were densely packed with multi-bacteroid symbiosomes (Fig. 6a and e). The host cell cytosol of metal-treated nodules was dense with large mitochondria in aggregates and plastids lacking starch grain. Poly-3-hydroxybutyrate (PHB) granules were absent in bacteroids of metal treated nodules (Fig. 6b-Dd) in contrast to the control ones (Fig. 6f-h). The most visible changes in nodules exposed to metals concerned cell walls. We observed in metal-treated nodules intense wall thickening of infected cells, especially in the cell corners (Fig. 6a-d). Such thick walls were not detected in the control nodules (Fig. 6e-h). The thick walls sometimes contained electron-dense precipitates (metal ions?) (Fig. 6b,d).

Apoplast changes in *L. corniculatus* nodules under metal stress

To reveal changes in the cell walls of *L. corniculatus* nodules under metal stress, epifluorescent microscopy was combined with cytochemical staining and immunocytochemical analysis with specific monoclonal antibodies against cell wall components (Fig. 7 and 8).

In metal treated nodules we saw thickened walls (Fig. 7) that contained more cellulose than control, as confirmed by intense staining with calcofluor white (Figs. 7b and 8b). The immunofluorescence localization of pectins (LM19 and LM20 antibodies), extensin (EXT) (LM1, JIM11 and JIM12), arabinogalactan protein (AGP) (LM2 and JIM13), xyloglucan (LM25) and callose revealed that these cell wall components were strongly induced during metal stress as compared with nonmetal treated nodules (Fig. 7 and 8). A comparative assessment of the degree of pectin methylation in nodule apoplast was carried out in this study using antibodies specific to high-methyl-esterified pectin (LM20 antibody) or low-methyl-esterified pectin (LM19). In metal-treated nodules intensely green fluorescent signal against both pectins (Fig. 7c,d) and EXT (Fig. 7e-g) was observed mainly in thickened walls. JIM11, JIM12 and LM1 EXT antigens were present in higher amounts in the cell walls and intercellular spaces of bacteroidal tissue and intercellular spaces of nodule parenchyma in metal treated nodules compare to control ones (Figs. 7e-g and 8e-g). Regarding

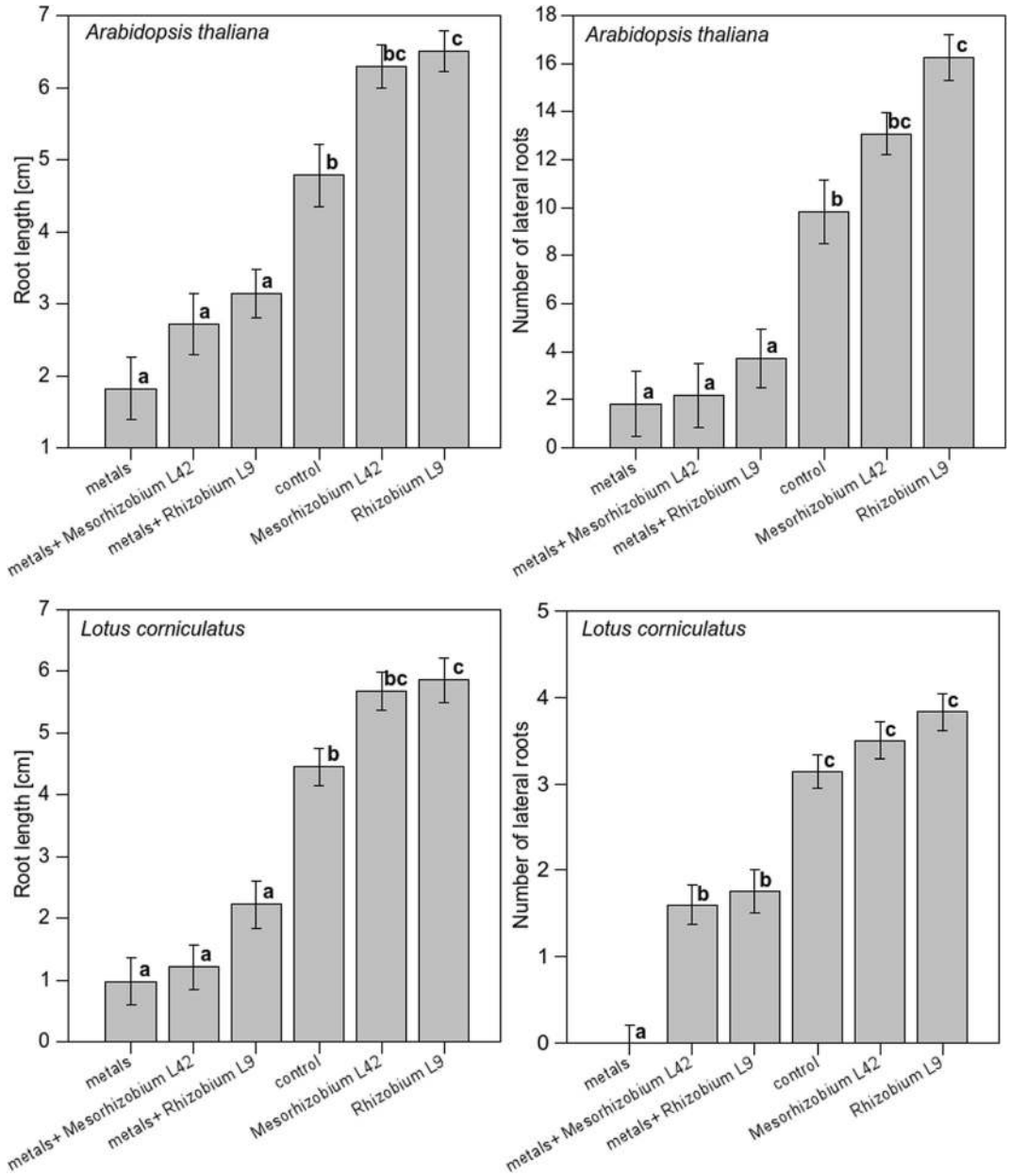

Fig. 3 Growth of *A. thaliana* and *L. corniculatus* plants on plates inoculated or not with L9 (*Rhizobium*) and L42 (*Mesorhizobium*) strains, growing in the presence or absence of Ni, Co and Cr. On graphs the values are means ± SD from two independent experiments. Control - non-inoculated plants. The same letters indicate the homogenous groups according to the Tukey HSD test at the level p=0.05

AGP, we studied distribution of epitopes in the nodules recognized by JIM13 and LM2 antibodies (Figs.7h, i and 8h, i). Interestingly, in metal treated nodules the AGP epitope recognized by LM2 antibody appeared not only in the thick cell wall but also in the cytoplasmic compartments of the infected cells (Fig. 7I). In control nodules (Fig. 8i), LM2 epitope labeled only cell walls of uninfected cells. In control nodules JIM13 strongly labeled only nodule endodermis (Fig. 8h), whereas in metal treated nodules JIM13 fluorescent signal was detected in cell wall and also in the cytoplasmic compartments of infected cells (Fig. 7h).

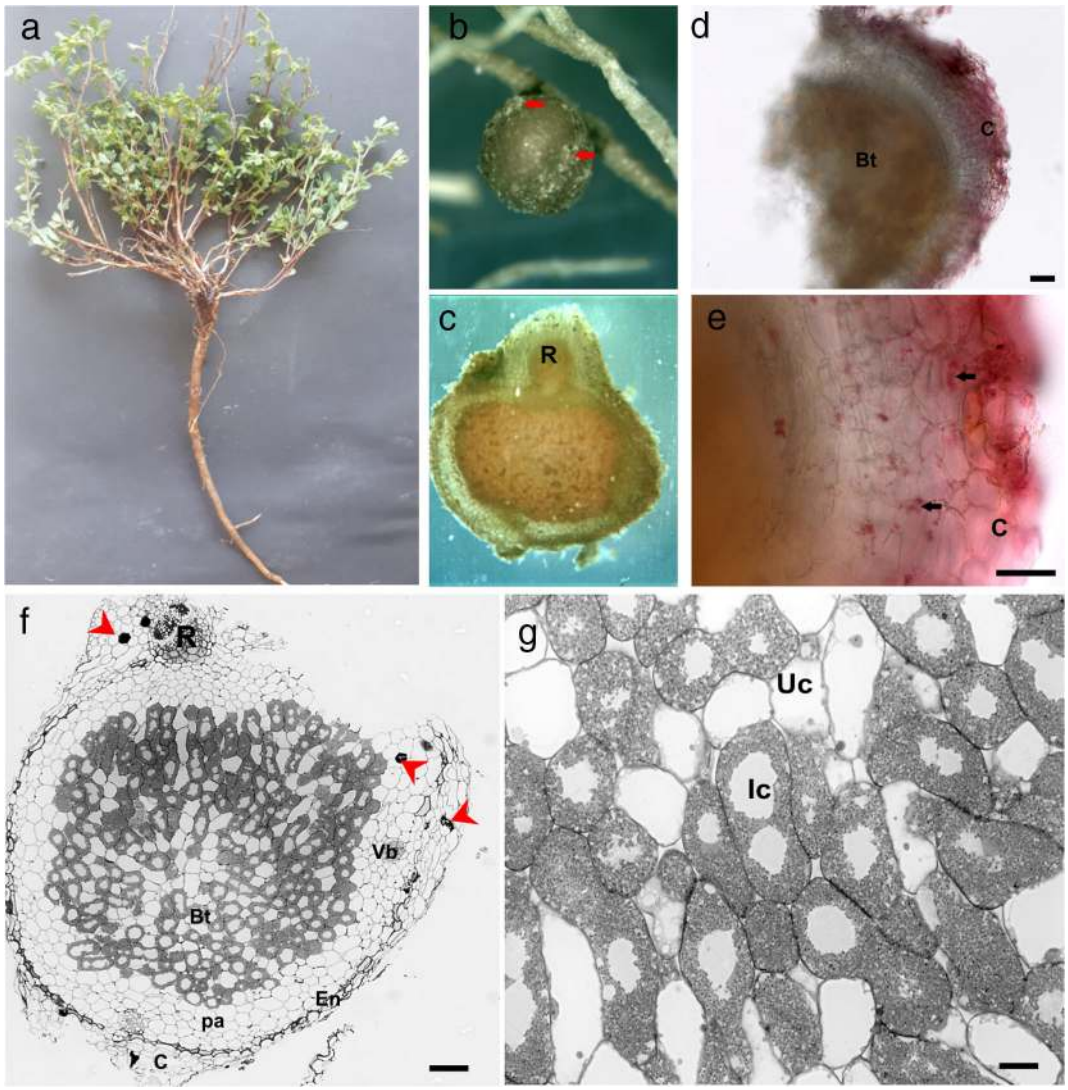

Fig. 4 **a** *L. corniculatus* plants growing on ultramafic mine spoil. **b** Visible birdsfoot trefoil nodule with stripe lenticles (arrows). **c** The interior of nodule revealing the red color of leghaemoglobin. **d**, **e**Ni detection with dimethylglyoxime in nodule cortex (c) as red color. **f**, **g** Light micrographs of fully developed determinate type of nodule, with central bacteroidal tissue (bt) with infected cells (Ic) with symbiosomes and uninfected cells (Uc) and periphery localized cortex tissues with nodule cortex (c), nodule endodermis (En) and nodule parenchyma (pa) with vascular bundles (vb). Visible phenolic inclusions (arrowhead) in nodule cortex tissues. **g** A light micrograph of nodule center with Ic with symbiosomes and Uc without starch grain. R – root. Scale bars = 20μm

LM25 strongly labeled thick walls of metal-treated nodules (Fig. 7j), whereas in control nodules the staining was less intense (Fig. 8j). In metal-treated nodules, a strong green fluorescence signal of callose was observed predominantly in plasmodesmata between the uninfected and infected cells (Fig. 7k), whereas a weaker signal was seen for these cells in control nodules (Fig. 8k). No green fluorescence signal was detected in any types of nodules without primary antibodies (Figs. 7l and 8l).

Discussion

As showed in this study, the ultramafic soil contained high amounts of Ni, Cr and Co, and Ni content was particularly high. Mean total content of Ni was over 48 times higher, and in the case of Cr and Co several times higher than in the soils of Europe (Salminen et al. 2005). The results of the soil extraction with 0.43 moldm^{-3} HNO_3 also revealed potentially high availability of Ni for ultramafic biota that can adversely affect both the

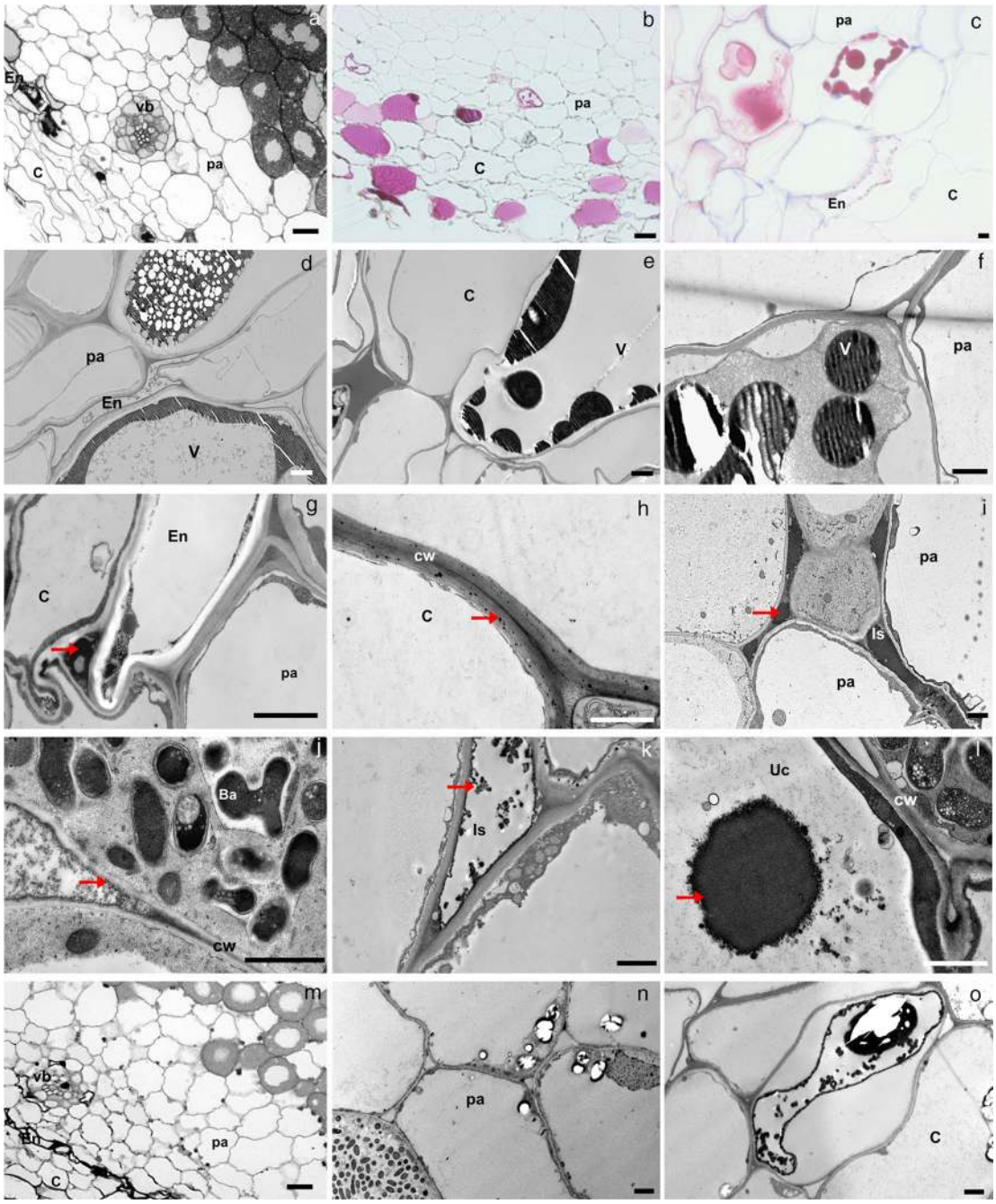

Fig. 5 LM and TEM micrographs of phenols in vacuoles and dark precipitates in metal-treated (A-L) and control (M-O) nodules. **a** Nodule cortex tissues: parenchyma (pa) cells with dark inclusion in intercellular spaces and dark nodule endoderma (En). **b**, **c** Phenolic vacuolar inclusions in the nodule cortex tissues stained in red with safranin. Scale bars = 50μm. **d**-**f** TEM micrographs of dark phenolic vacuolar inclusions in nodule cortex tissues. **g**-**l** TEM micrographs of dark precipitates (metal ions?) (arrow) in intercellular spaces of cortex tissues (**g**-**i**), in cell wall (**h**) and bacteroidal tissue (**j**, **k**). **l** Visible dark precipitates (arrow) in central vacuole of uninfected cells. **m** LM control nodule with cortex tissues. Scale bars = 50 μm. **n**, **o** Control nodule and visible lack of dark precipitates in the nodule endoderma, intercellular spaces (Is) of cortex tissue and sporadic phenols accumulation in the vacuoles of the nodule cortex. Ba - bacteroid; c- nodule cortex; cw - cell wall; En - nodule endoderma; Uc- uninfected cell; pa- nodule parenchyma; v - vacuole; vb- vascular bundle. Scale bars = 2μm

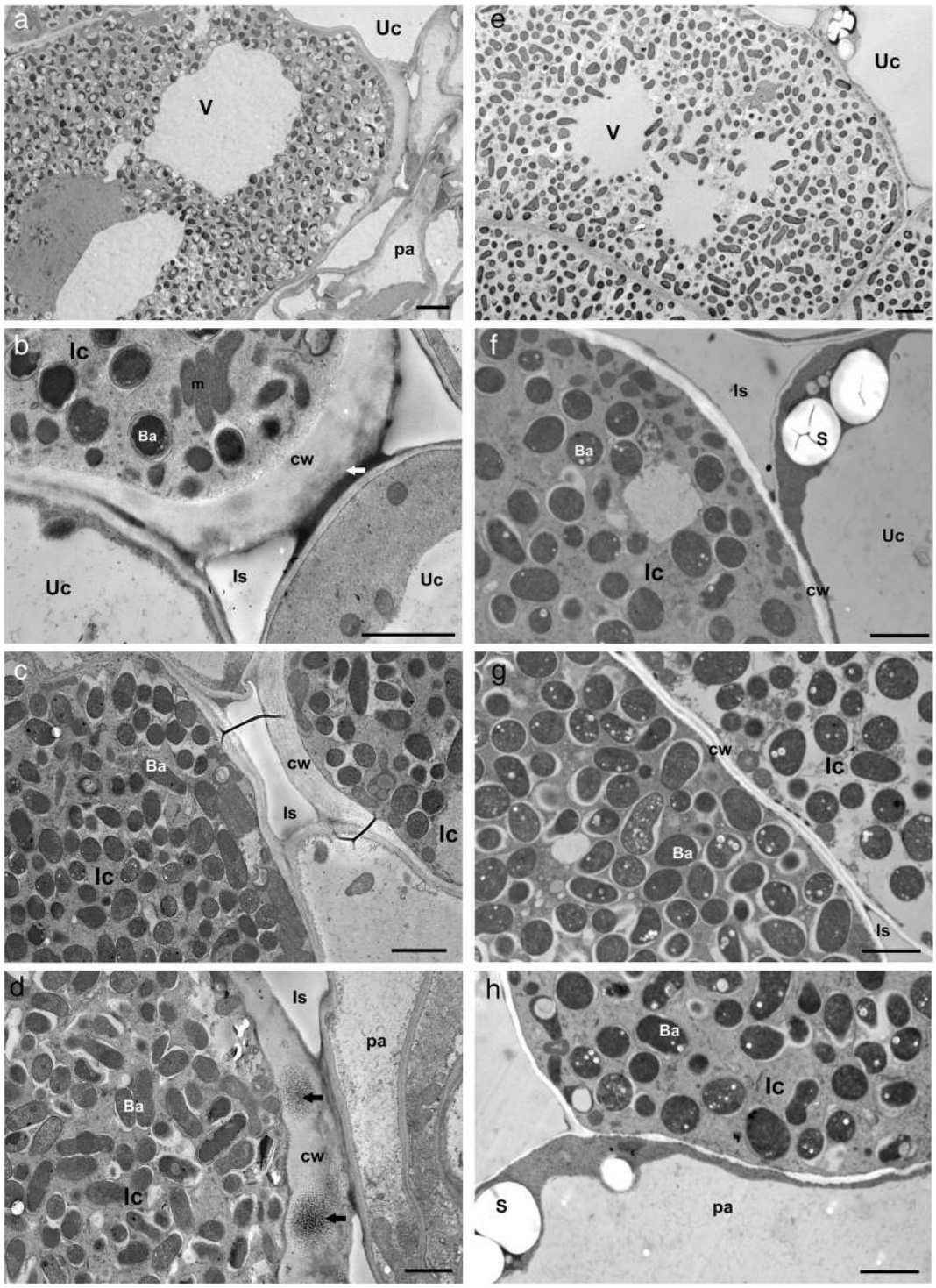

Fig. 6 Bacteroidal tissue and cell walls of infected cells of metal-treated (**a**-**d**) and control (**e**-**h**) *Lotus corniculatus* nodules. **a** Visible two enlarged central vacuoles (v) of infected cells. **b**-**d** Visible wall thickening of infected cells (Ic) corners: between Ic and uninfected cell (Uc) (**b**), between neighboring Ic (**c**), and between Ic and nodule parenchyma (pa) (**d**). Thickened walls local contain dark precipitates (arrows) (metal ions?). **e** Visible small vacuoles (v) in IC of control nodule. **f**-**h** Visible thin walled Ic with symbiosomes with small grains of poly-3-hydroxybutyrate. The uninfected cells and parenchyma cells contain large starch grain (S). Ba - bacteroid; cw- cell wall; m - mitochondrion; Is - intercellular space. Scale bars = 2 μm

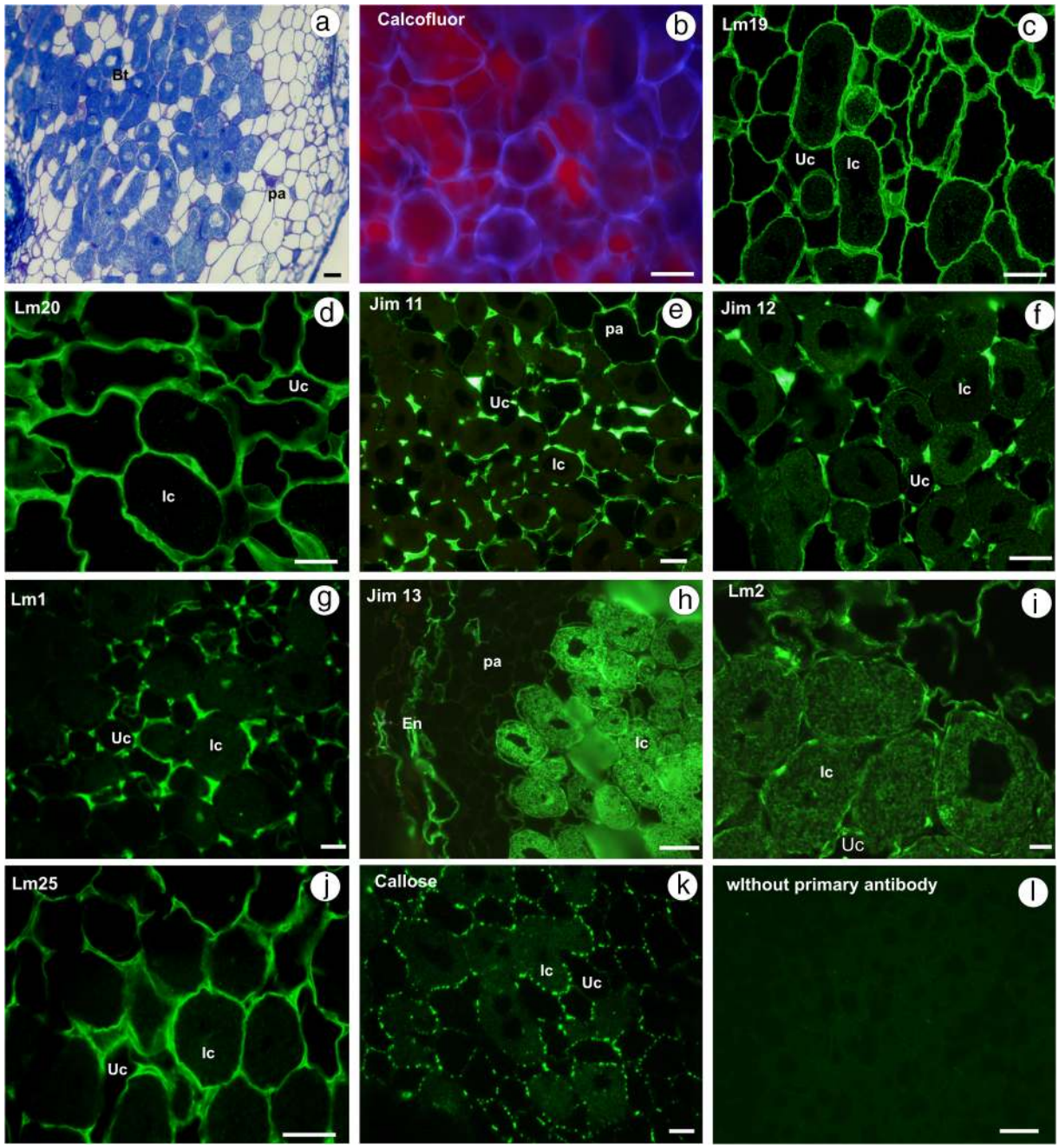

Fig. 7 Cytochemical and immunofluorescence localization of cell wall components in metal-treated nodules of *L. corniculatus*. **a** Light microghraphs of central part of nodule stained with toluidine blue. Visible bacteroidal tissue (Bt) with infected and uninfected cells surrounded by nodule parenchyma (pa). **b** Calcofluor white fluorescence of cellulose is shown in blue. (C-K) Strong fluorescence signal in serpentine nodules using monoclonal antibodies against non-cellulosic wall components. (L) Visible lack of green fluorescence signal when primary antibodies were omitted. En- nodule endoderma; IC – infected cell; Uc- uninfected cell. Scale bars = 20μm

plants and the microorganisms. The importance of Cr and Co as potentially harmful elements seems to be much smaller than Ni because of their lower contents and less mobility. This obtained sequence of the metal extractability (Ni>Co>Cr) usually occurs in the ultramafic soils (Kazakou et al. 2008; Kumar and Maiti

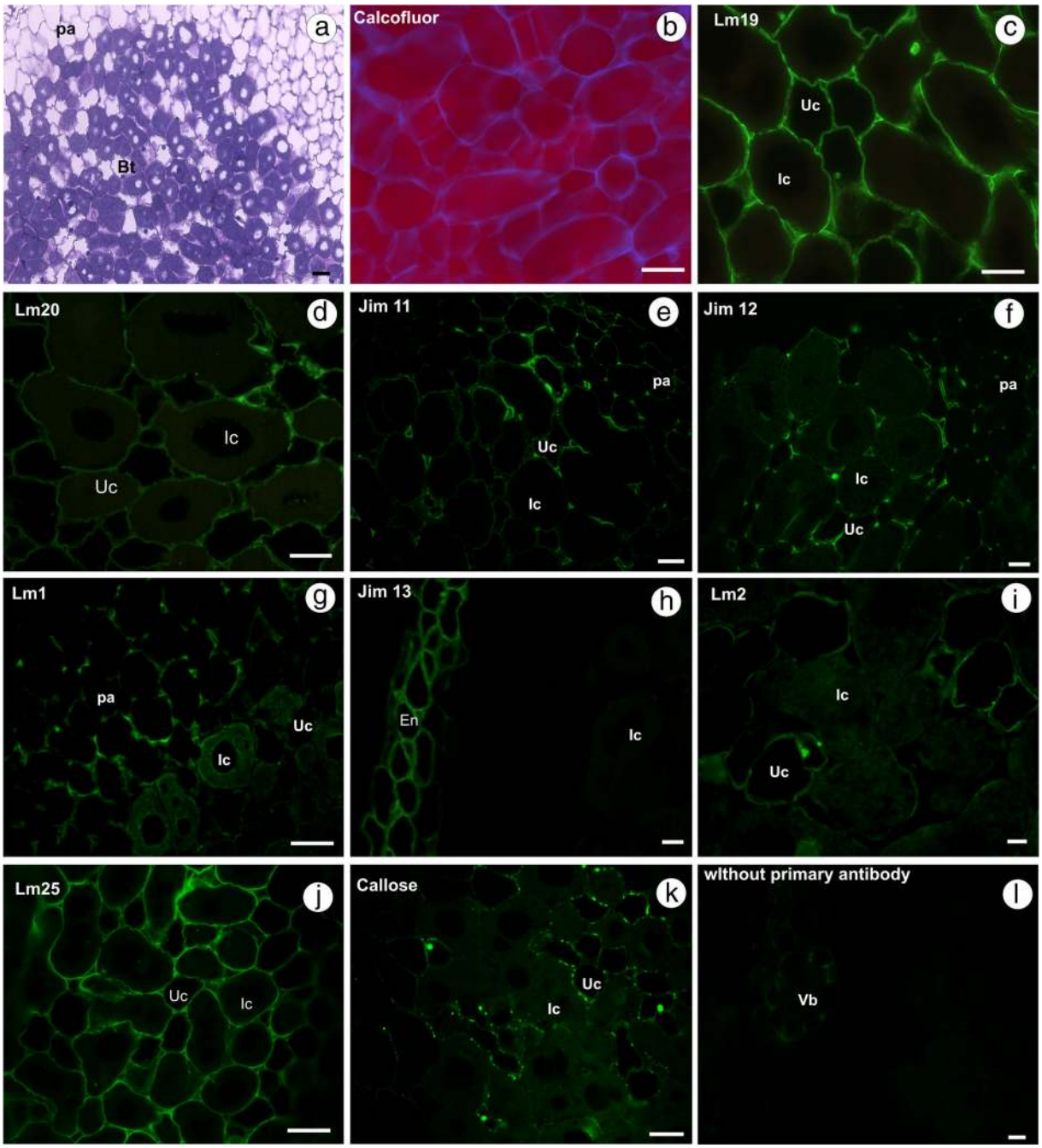

Fig. 8 Cytochemical and immunofluorescence localization of cell wall components in control nodules of *L. corniculatus*. **a** Light microghraphs of central part of nodule stained with toluidine blue. Visible bacteroidal tissue (Bt) with infected and uninfected cells surrounded by nodule parenchyma (pa). **b** Calcofluor white fluorescence of cellulose is shown in blue. **c**-**k** Weak immunostaining of non-cellulosic wall components in control nodules. **l** Visible lack of green fluorescence signal when primary antibodies were omitted. En - nodule endoderma; IC - infected cell; Uc- uninfected cell; vb- vascular bundle. Scale bar= 20μm

2013; Kierczak et al. 2016). In comparison with other studies of ultramafic soils from the Szklary Massif, the total form levels of Ni and especially Cr were lower than obtained by other researches (Żołnierz 2007; Kierczak et al. 2016). These differences, as well as high variability of the elements content among samples, were

probably mostly due to the specificity of the sampling substrate which, as the mine or smelt waste material, did not derive from the natural ultramafic outcrops with an undisturbed soil profile but were anthropogenically transformed.

Our analysis of metal content in plant organs and TF values confirmed a tendency to Ni, Cr and Co accumulation in the roots and their low translocation ability to the shoots, which suggest *L. corniculatus* exclusion strategy of dealing with these metals. The shoots accumulated 59.5 mg kg^{-1} d.w. of Ni, 5.4 mg kg^{-1} d.w. of Cr and 2.4 mg kg^{-1} d.w. of Co, and these values are much higher than the normal concentrations in plants (Markert 1994). According to Kabata-Pendias (2010), toxic levels of these metals in shoots reach 10-100 mg kg^{-1} d.w. for Ni, 1-2 mg kg^{-1} d.w. for Cr and 30-40 mg kg^{-1} d.w. for Co. The roots accumulated Ni, Cr and Co at 167.1, 20.5 and 8.5 mg kg^{-1} d.w., respectively. Despite the fact that Ni and Cr content in the plant shoots exceeded their toxic values, no toxicity symptoms were observed. The translocation factor revealed *L. corniculatus* tolerance strategy to high levels of toxic metals as its values fell below 1 for all studied elements. Such a defense strategy is common for metal-tolerant plants (Baker and Brooks 1989). Our results confirmed earlier findings concerning this species from ultramafic soil reported by Pędziwiatr (2018). The plants restraining metals in roots accumulate them in root endodermis and cortical tissues (Parrota et al. 2015). In our study, the presence of Ni in *L. corniculatus* nodules was confirmed by histochemical staining with dimethylglyoxime and revealed the nodule ability to Ni accumulation in their cortex tissues. Gopalakrishnan et al. (2015) reported that at metal contaminated sites nodules may be the main spots of metal accumulation.

Although *L. corniculatus* is native to several countries in Europe and is a pioneer plant on metal polluted sites, very few studies have explored diversity of its symbiotic partner on ultramafic soils (Mengoni et al. 2010; Escaray et al. 2012; Lorite et al. 2018). In this work, the preliminary characterization of the *L. corniculatus* nodulated rhizobia was conducted using partial sequences of two housekeeping genes (*glnII* and *dnaK*). BLASTn and Blast Microbes searches revealed a phylogenetic affinity within the genera *Rhizobium* and *Mesorhizobium*. Four strains represented *M. septentrionale* – a species reported in the nodules of *L. corniculatus* plants growing in non-metal contaminated Norwegian soils (Gossmann et al. 2012). There is also a report concerning *R. leguminosarum* isolated from bird's foot trefoil nodules from Swedish soils (Apomah and Huss-Danell 2011). Most importantly, this work uncovered a novel lineage within the genus *Rhizobium,* and presumably also a new metal-resistant species in the genus *Mesorhizobium*. These strains will be subjected to further, more detailed phylogenetic and genomic characterization.

Studies on ultramafic soils indicated that only a small group of rhizobia inhabiting nickel-contaminated soils developed resistance mechanisms against this toxic metal (Pereira et al. 2006; Abou-Shanab et al. 2007; Pal et al. 2007; Chaintreuil et al. 2007; Fagorzi et al. 2018). In our study, *Rhizobium* (L9, L19) and *Mesorhizobium* (L42 and L50) strains most effective in nodulation on ultramafic soils showed multi metal tolerance. They were tolerant not only to Ni (up to 0.2 mM), but also to Co and Cr (up to 5 mM). Schmidt and Schlegel (1994) showed that regarding the Co and Ni resistances, it is frequent the appearance of multiresistance since the nickel-cobalt resistance genes are carried by the same plasmid. A recent Porter et al. (2017) genome-wide association study identified candidate genes for adaptation of *Mesorhizobium* strains to nickel in ultramafic soils. Delorme et al. (2003), Pereira et al. (2006) and Rubio-Sanz et al. (2018) reported that *R. leguminosarum* bv. *viciae* isolated from metal polluted sites exhibited abroad spectrum of metal resistance. In our study, we observed an increased growth of *R. leguminosarum* and *M. septentrionale* at the intermediate Co and Cr doses. It would suggest the high tolerance of these strains to these metals. Similar stimulation effect of medium metal doses on rhizobia growth was observed in our previous studies (Sujkowska-Rybkowska and Ważny 2018; Sujkowska-Rybkowska et al. 2020). Delorme et al. (2003) indicated that in polluted soils, the tolerance of bacteria to one or more metals may be due to the existence of distinct, independent metal tolerance mechanisms in their organisms. Other reports show a presence of metal tolerating *Bradyrhizobium* (Wani et al. 2007), *R. leguminosarum* (Rubio-Sanz et al. 2018) and *Mesorhizobium* strains isolated from nodules of legume plants growing on nickel contaminated soils (Porter and Rice 2013). It has been suggested that rhizobia possess different Ni-tolerance systems (Chaintreuil et al. 2007; Fagorzi et al. 2018). Several studies show that bacteria inhabiting ultramafic soils developed different metal tolerance mechanisms to maintain low intracellular metal

concentrations (Chaintreuil et al. 2007; Haferburg and Kothe 2007; Zielazinski et al. 2013). Rhizobial exo- and lipopolysaccharides influence metal resistance by forming complexes with metal ions through electrostatic interactions (Liu et al. 2001). *Ensifer, Mesorhizobium* and *Bradyrhizobium* strains have active Ni efflux systems (Chaintreuil et al. 2007; Zielazinski et al. 2013). Some highly tolerant *R. leguminosarum* strains accumulate metals in intracellular spaces (Purchase et al. 1997; Purchase and Miles 2001; Pereira et al. 2006). *Mesorhizobium* bacteria have active Ni efflux systems to prevent toxic intracellular nickel concentrations (Maynaud et al. 2013). On the other hand, rhizobia survival in metal contaminated soil can be related to physical protection of organic matter and clay minerals (Ibekwe et al. 1997; Giller et al. 1998) or to the existence of specific "niches" in the soil such as root nodules, where metal contamination may be minimal.

Our study indicated that apart from metal resistance isolated strains of *Rhizobium* (L9, L19) and *Mesorhizobium* (L42 and L50) exhibited high PGP abilities under metal (Ni, Co or Cr) presence (Table 5). These strains were capable of producing high amounts of auxin and siderophore and showed phosphate solubilizing ability under metal stress. Many reports have provided evidence that nodulating rhizobia may induce plant growth directly by nitrogen fixation, phosphate solubilization, siderophore or phytohormone synthesis and ACC deaminase production (Stearns et al. 2005; Ma et al. 2011; Gopalakrishnan et al. 2015; Karthik et al. 2017). Rhizobial PGP traits improving growth of legumes in metal contaminated soils were observed for *Bradyrhizobium* under Cd stress (Guo and Chi 2014), and *Rhizobium* nodulating *Prosopis juliflora* on metal-contaminated soil (Rai et al. 2004). Wani et al. (2008) showed similar effects of *Mesorhizobium* strain on chickpea grown in Cr contaminated soils. Phosphorus solubilization was reported for *Rhizobium sp., and Mesorhizobium sp.* (Vessey 2003; Gopalakrishnan et al. 2015). *Rhizobium, Sinorhizobium and Bradyrhizobium sp.* are known to produce siderophores (Carson et al. 2000; Arora et al. 2001). It therefore seems that Rhizobium and Mesorhizobium strains may improve *L. corniculatus* growth and increase plant stress tolerance on ultramafic soils.

In this study, we also showed a direct promotional effect of *R. leguminosarum* bv. *viciae* (L9) and *M. serpentionale* (L42) on *L. corniculatus* and non-legume *Arabidopsis thaliana* (Fig. 3). Seedling root growth and lateral root formation in *A. thaliana* and host plants was promoted by inoculation with both strains, especially under metal presence. Our findings confirmed the tests for PGP abilities of isolated rhizobia and indicated the existence of beneficial interactions of rhizobia not only with legume plants. Apart from the ability to form nitrogen-fixing symbiosis with legumes, many rhizobia are known to develop growth promoting associations with non-legumes, such as maize, rice (Gutiérrez-Zamora and Martínez-Romero 2001; Ladha and Reddy 2003), and *Arabidopsis* (Zhao et al. 2017). In metal contaminated soil rhizobia may be an important microflora not only for their host but also for neighboring plants growing in these difficult conditions.

The ultramafic legumes should have specific mechanisms of tolerance and adaptation to these soil conditions, the more so because there is a strong evidence from pot experiments that some metals, especially Ni, affect nitrogen fixation in legume nodules and significantly limit their yield (Athar and Ahmad 2002). To understand possible adaptive mechanisms of *Lotus*-rhizobia symbiosis under metal stress it is necessary to determine cellular organization of the symbiotic nodules. However, there are few studies that discuss the effects of toxic metals on nodule structure and functioning at their natural sites (Ibekwe et al. 1995; Wani and Khan 2013; Sujkowska-Rybkowska and Ważny 2018). Nodules represent a unique environmental niche for symbionts accommodation and proliferation by providing microsites in metal-contaminated soils where toxic influence of metal ions is limited. In this study, we show that Ni is detained in ultramafic nodule cortex tissue, which was shown with dimethylglyoxime dyeing. Interestingly, in this study electron microscope analysis revealed structural alterations (wall thickening and phenols accumulation) in the ultramafic *L. corniculatus* nodules that may prevent negative effects of metals on the symbiosis. We found clear differences in the structure between control and metal-treated nodules. *L. corniculatus* under control and metal stress conditions formed determinate nodules typical of the tribe Loteae (Brewin 1991). The central part of nodules accounted bacteroidal tissue with uninfected and infected cells with bacteroids. We noted that the bacterial conversion to bacteroids in metal-treated *L. corniculatus* nodules was associated with a lower PHB accumulation compare to control nodules. A similar PHB decrease was observed in *L. corniculatus* nodules after forage harvest (Vance et al. 1982). In metal-treated nodules infected and uninfected cells were devoid of starch granules. Lower starch accumulation in nodules exposed to metals could be a result of low C supply from the plant to

the nodule caused by metal stress since photosynthesis is impaired by metals (Paunov et al. 2018). The ultramafic and control nodules were surrounded by a multilayer cortex consisting of parenchyma for gas diffusion, endodermis for ion transport and outer cortex serving as a barrier against pathogens and toxic ions (Brewin 1991). The vacuoles of the nodule endodermis and some cortical and parenchymal cells were filled with dark phenolic substances, the nature of which was confirmed by safranin staining (Broda 1971). These phenolic vacuolar inclusions could be flavolans (condensed tannins) that are naturally accumulated in *L. corniculatus* nodules (Monza et al. 1992). In metal treated nodules we observed increased number of cortex cells filled with tannins. The adaptation of *L. corniculatus* plants to metal stress could be attributed to enhanced synthesis of phenolic compounds. The protective role of phenols against toxic metals consisting in metal chelation and scavenging harmful reactive oxygen species generated in the presence of toxic ions is well known (Sharma et al. 2012). Lafuente et al. (2015) revealed the induction of the synthesis of phenolic compounds (phenylpropanoids, isoflavonoids) in nodules of *Medicago* plants in the presence of arsenic. Recent studies of Raklami et al. (2019) showed that in nodules of *M. sativa* plants inoculated with metal resistant strains and cultivated in the presence of metals the gene coding phenylalanine ammonia lyase is expressed. This enzyme is the start point of two important pathways: secondary metabolism of phenolic compounds and lignin synthesis.

In ultramafic nodules we noted significant wall thickening of the infected cells, especially in their corners. Plant cell wall is the first barrier against toxic metals and cell wall construction is very important in plant resistance to abiotic stress (Le Gall et al. 2015). The cell wall structure comprising cellulose microfibrils and non-cellulosic neutral polysaccharides embedded in pectin matrix with proteins and phenolic compounds, confers metal binding ability (Probst et al. 2009; Krzesłowska 2011). Cell wall thickening is one of metal exclusion strategy in plants, and apoplast (cell walls and intercellular spaces) is the main site of toxic ion sequestration (Zornoza et al. 2002; Krzesłowska 2011). Thickening of the cell wall helps to increase mechanical strength and raises its binding capacity of metal ions thus preventing their entry into the protoplast (Krzesłowska 2011; Le Gall et al. 2015). This leads to modifications in cell wall structural properties (Krzesłowska 2011; Le Gall et al. 2015). In our experiment, some precipitates visible in metal-treated nodule apoplast could be metal ions sequestrated in the walls and intercellular spaces. However, such metal distribution should be confirmed by more advanced techniques, such as Energy Dispersive X-ray (EDX) microanalysis or X-ray fluorescence (XRF) imaging, which are planned at further stages of our research.

We used immunohistochemical method with different antibodies directed against wall components to analyze changes in the nodules cell wall composition under metal stress. We observed apoplast remodeling in metal-treated nodules, which may be considered as indicators of adaptation strategy of *L. corniculatus*–rhizobia symbiosis to metal stress conditions. Cell walls of metal-treated nodules were thickened and contains more cellulose and hemicellulose compare to control nodules, as indicated by dyeing with calcofluor and LM25 antibody labelling (Figs.6-8). The higher deposition of these wall components is commonly observed in thick secondary walls (Le Gall et al. 2015). Recent studies of Tsyganova et al. (2019) revealed that highly methylesterified pectins (detected by JIM7 and LM20 antibodies) showed a uniform localisation in the cell walls of non-metal treated M. truncatula and Pisum sativum nodules, whereas low methylesterified pectins recognised by JIM5 and LM19 localized mainly in the walls of infection threads. In this study, in metal-treated nodules thickened walls of infected cell, especially their corners, were intensively labelled with pectins antibodies (LM19 and LM20). The increase of pectins, especially low-methylesterified in walls of metal treated roots (Krzesłowska 2011) and nodules (Sujkowska-Rybkowska and Borucki 2015) was often observed. Pectins together with hemicellulose play important role in metals binding (Krzesłowska 2011; Le Gall et al. 2015). Wall thickenings might be a result from stiffening of the polysaccharide network. De-esterified pectins can be cross-linked by calcium ions or metal ions what impacting on cell wall mechanical properties and metal immobilization (Krzesłowska 2011). In our studies, in addition to pectins the thick walls of infected cells of metal-treated nodules contains also higher amount of EXT (recognized by LM1, JIM11 or JIM12 antibodies) compare to control. Additionally, intercellular spaces of uninfected cell and cortex tissue of metal-treated nodules were significantly filled with these structural glycoproteins. EXTs are responsible for cell wall stiffening (Kieliszewski and Lamport 1994). In root nodules, this glycoproteins intercellular localization in nodule parenchyma play role as diffusion barrier that helps protects nitrogenase from inactivation (Vanden Bosch et al. 1989; Rathbun et al. 2002). Similar occlusions in the intercellular spaces have been reported in nodules under

different stresses (de Lorenzo et al. 1993; Iannetta et al. 1995; Sujkowska-Rybkowska and Borucki 2014). Such modifications might render cell walls less permeable to metals thus limiting its entry in the cell interior and bacteroidal tissue. In present study thick walls and cytoplasmic compartments of infected cells of metal treated nodules show also presence of AGP (recognized by LM2 antibody). Such AGP cytoplasmic localization may indicate an extensive internal membrane system (Šamaj et al. 2000). LM2 epitope is closely associated with endomembranes of the endoplasmic reticulum, Golgi apparatus and tonoplast of different plant cells (Šamaj et al. 2000). These glycoproteins are involved in different cellular and developmental processes and response to different biotic and abiotic stresses (Lamport et al. 2006). AGPs may be transported as a compartments of the endomembrane flow participating in AGP exocytosis to apoplast, where AGP play role as pectin plasticizers (Lamport et al. 2006). AGP may reducing the formation of pectate gels and affecting cell wall extension (Serpe and Nothnagel 1994). AGPs are also localized in the infected cells of legume nodules and play an essential role in symbiotic tissue (Cassab 1986; Fruhling et al. 2000). In pea nodules, the only other nodule examined to date, JIM13 epitope recognized AGP was associated with nodule lignified endoderma (Rae et al. 1991). Surprisingly, metal treated *L. corniculatus* nodules also showed increased amount of AGP recognized by JIM13 antibody not only in nodule endodermis but also in cytoplasmic compartments of infected cells. This may indicate the presence of new bacteroidal tissues-specific AGP epitopes under metal stress. Metal treatment also induced in nodules accumulation of callose in plasmodesmata between infected and uninfected cells. Callose regulates the plasmodesmata permeability and limits metal ions movement into the cytoplasm (O'Lexy et al. 2018). Taking together, the results suggest that *L. corniculatus* nodules respond to Ni, Cr and Co with changes in the cell wall components (celullose, hemicellulose, pectins, EXT, AGP and callose), which may limit the influx of harmful ions to the cytoplasm of infected cells with symbiosomes and act protectively on *L. corniculatus*-rhizobia symbiosis in the presence of these metals.

Conclusions

Our results indicate for the first time that *L. corniculatus* nodules are inhabiting by beneficial metal-tolerant, growth promoting rhizobacteria, which have the potential to improve plant growth and alleviate Ni, Cr and Co stress on ultramafic soils**.** In addition, in these nodules, the accumulation of phenols and remodeling of apoplast can counteract the harmful effects of these metals on both bacterial symbiont and host. These findings imply that *L. corniculatus*-rhizobia symbiosis is an important element of plant adaptation to the metal stress occurring on ultramafic soils.

Acknowledgments The authors thank the Ministry of Science and Higher Education of the Republic of Poland for partial financing of the research. The immunocytochemical analysis with specific antibodies against cell wall components was financially supported by the Polish National Science Centre within the project no. DEC-2019/03/X/NZ9/00019.

Authors' contributions Conceptualization MS-R; MS-R wrote the manuscript, sectioned material for microscopy, did microscopic observations, digital documentation and its analysis; DK collected plants and seeds, revised the manuscript and with KG performed chemical analysis; MS-R isolated bacteria and did its metal tolerance and PGP traits analyses; JB and TS did molecular identification of bacteria.

References

Abou-Shanab RI, Berkum P, Angle JS (2007) Heavy metal resistance and genotypic analysis of metal resistance genes in gram-positive and gram-negative bacteria present in Ni-rich serpentine soil and in the rhizosphere of *Alyssum murale*. Chemosphere 68(2):360–367

Ahmad MS, Ashraf M (2011) Essential roles and hazardous effects of nickel in plants. Rev Environ Contam Toxicol 214:125–167

Aka RJN, Babalola OO (2017) Identification and characterization of Cr-, Cd-, and Ni-tolerant bacteria isolated from mine tailings. Bioremed J 21(1):1–19

Alexander EB (2004) Serpentine soil redness, differences among peridotite and serpentinite materials, Klamath Mountains, California. International Geology Review 46:754–764

Alexander ADB, Zuberer DA (1991) Use of chrome azurol S reagents to evaluate siderophore production by rhizosphere bacteria. Biol Fert Soils 12:39–45

Altschul SF, Gish W, Miller W, Myers EW, Lipman DJ (1990) Basic local alignment search tool. J Mol Biol. 215(3):403–410

Apomah OY, Huss-Danell K (2011) Genetic diversity of root nodule bacteria nodulating *Lotus corniculatus* and *Anthyllis vulneraria* in Sweden. Syst Appl Microbiol 34(4):267–275

Arora NK, Kang SC, Maheshwari DK (2001) Isolation of siderophore-producing strains of *Rhizobium meliloti* and their biocontrol potential against *Macrophomina phaseolina* that causes charcoal rot of groundnut. Curr Sci 81(6):673–677

Athar R, Ahmad M (2002) Heavy metal toxicity in legume microsymbiont system. J Plant Nutri 25:369–386

Baker AJM, Brooks RR (1989) Terrestrial higher plants which hyperaccumulate metallic elements. Biorecovery1:81–126

Banuelos G, Cardon G, Mackey B, Ben-Asher J, Wu L, Beuselinck P (1992) Boron and selenium removal in boron-laden soil by birdsfoot trefoil. J Environ Quality 22(4)

Benson DA, Karsch-Mizrachi I, Lipman DJ, Ostell J, Wheeler DL (2005) GenBank. Nucleic Acids Res 33(Database issue): D34–D38

Beukes CW, Stępkowski T, Venter SN, Cłapa T, Phalane FL, le Roux MM, Steenkamp ET (2016) Crotalarieae and Genisteae of the South African great escarpment are nodulated by novel *Bradyrhizobium* species with unique and diverse symbiotic loci. Mol Phylogenet Evol 100:206–218

Bhalerao SA, Sharma AS, Poojari AC (2015) Toxicity of nickel in plants. Int J Pure App Biosci 3(2):345–355

Blumenthal M, McGraw R (1999) *Lotus* adaptation, use and management. In: Trefoil: The science and technology of *Lotus*. Beuselinck P, (ed.) American Society of Agronomy, pp. 97-120.

Brady KU, Kruckeberg AR, Bradshaw HD (2005) Evolutionary ecology of plant adaptation to serpentine soils. Ann Rev Ecol Evolut System 36:243–266

Brewin NJ (1991) Development of the legume root nodule. Ann Rev Cell Biol 7:191–226

Broda B (1971) Methods of plant histochemistry (in Polish). PWZL, Warsaw

Brooks RR (1987) Serpentine and its vegetation: a multidisciplinary approach. Dioscorides Press, Portland, Oregon

Carson KC, Meyer J, Dilworth MJ (2000) Hydroxamate siderophores of root nodule bacteria. Soil Biol Biochem 32: 11–21

Cassab G (1986) Arabinogalactan proteins during the development of soybean root nodules. Planta 168:441–446

Chaintreuil C, Rigault F, Moulin L, Jaffre T, Fardoux J, Giraud E (2007) *Nickel resistance determinants in Bradyrhizobium strains from nodules of the endemic New Caledonia legume Serianthes calycina*. Appl Environ Microbiol 73:8018–8022

Chaudri AM, McGrath SP, Giller KE, Rietz E, Sauerbeck DR (1993) Enumeration of indigenous *Rhizobium leguminosarum* biovar *trifolii* in soils previously treated with metal-contaminated sewage sludge. Soil Biol Biochem 25:301–309

Coleman R.G. (1971) Petrologic and geophysical nature of serpentinites. Geological Society of America Bulletin. 87: 897–918

Davies PJ (2010) The Plant Hormones: Their nature, occurrence and functions. 3rd ed. New York: Kluwer Academic Publishers; pp. 656.

de Lorenzo C, Iannetta PPM, Fernández Pascual MF, De Felipe MR (1993) Oxygen diffusion in lupin nodules: II. Mechanisms of diffusion barrier operation. J Exp Bot 44(266):1469–1474

de los Santos G, Steiner JJ, Beuselinck PR (2001) Adaptive ecology of *Lotus corniculatus* L. Genotypes: II. Crossing ability. Crop Sci 41(2):564–570

Delorme TA, Gagliardi JV, Angle JS, van Berkum P, Chaney RL (2003) Phenotypic and genetic diversity of Rhizobia isolated from nodules of clover grown in a zinc and cadmium contaminated soil. Soil Sci Soc Am J 67(6)

Escaray FJ, Menendez AB, Gárriz A, Pieckenstain FL, Estrella MJ, Castagno LN, Carrasco P, Sanjuán J, Ruiz OA (2012) Ecological and agronomic importance of the plant genus *Lotus*. Its application in grassland sustainability and the amelioration of constrained and contaminated soils. Plant Sci 182:121–133

Evans BW, Hattori K, Baronnet A (2013) Serpentinite: What, why, where? Elements 9(2):99–106

Fagorzi C, Checcucci A, diCenzo GC, Debiec-Andrzejewska K, Dziewit L, Pini F, Mengoni A (2018) Harnessing Rhizobia to Improve Heavy-Metal Phytoremediation by Legumes. Genes 9(11):542

Franzini VI, Azcón R, Latanze-Mendes F, Aroca R (2010) Interaction between *Glomus* species and *Rhizobium* strains affect the nutritional physiology of drought stressed legume hosts. J Plant Physiol 167:614–619

Fruhling M, Hohnjec N, Schroder G, Kuster H, Puhler A, Perlick AM (2000) Genomic organization and expression properties of the VJENOD5 gene from broad bean (*Vicia faba* L.). Plant Sci 155: 169–178

Gerendás J, Polacco JC, Freyermuth SK, Sattelmacher B (1999) Significance of nickel for plant growth and metabolism. J Plant Nutr Soil Sci 162:241–256

Giller KE, Witter E, McGrath SP (1998) Toxicity of heavy metals to microorganisms and microbial processes in agricultural soils. Soil Biol. Biochem. 30: 1389–1414

Giller KE, Witter E, McGrath SP (2009) *Heavy metals and soil microbes*. Soil Biol Biochem 41:2031–2037

Gopalakrishnan S, Sathya A, Vijayabharathi R, Varshney RK, Gowda CLL, Krishnamurthy L (2015) Plant growth promoting rhizobia: challenges and opportunities. Biotech 5:355–377

Gossmann JA, Markmann K, Brachmann A, Rose LE, Parniske M (2012) Polymorphic infection and organogenesis patterns induced by a *Rhizobium leguminosarum* isolate from *Lotus* root nodules are determined by the host genotype. New Phytol 196(2):561–573

Groenenberg JE, Römkens PFAM, van Zomeren A, Comans RNJ (2017) Evaluation of the single dilute (0.43 M) nitric acid extraction to determine geochemically reactive elements in soil. Environ Sci Technol. 51(4):2246–2253

Gruber N, Galloway JN (2008) *An Earth-system perspective of the global nitrogen cycle*. Nature 451:293–296

Guo JK, Chi J (2014) Effect of Cd-tolerant plant growth-promoting rhizobium on plant growth and Cd uptake by *Lolium multiflorum* (L.) and *Glycine max* (L.) in Cd-contaminated soil. Plant Soil 375:205–214

Gutiérrez-Zamora ML, Martínez-Romero E (2001) Natural endophytic association between *Rhizobium etli* and maize (*Zea mays* L.). J Biotechnol 91:117–126

Haferburg G, Kothe E (2007) Microbes and metals: interactions in the environment. J Basic Microb 47:453–467

Hao X, Taghavi S, Xie P, Orbach MJ, Alwathnani HA, Rensing C, Wei G (2014) Phytoremediation of heavy and transition metals aided by Legume-Rhizobia Symbiosis. Int J Phytorem 16(2):179–202

Hardy RWF, Holsten RD, Jackson EK, Burns RC (1968) The acetylene – ethylene assay for N_2 fixation: laboratory and field evaluation. Plant Physiol 43:1185–1207

Iannetta PPM, James EK, Sprent JI, Minchin FR (1995) Time-course of changes involved in the operation of the oxygen diffusion barrier in white lupin nodules. J Exp Bot 46:565–575

Ibekwe AM, Angle JS, Chaney RL, van Berkum P (1995) Sewage sludge and heavy metal effects on nodulation and nitrogen fixation of legumes. J Environ Qual 24:1199–1204

Ibekwe AM, Angle JS, Chaney RL, van Berkum P (1997) Enumeration and N fixation potential of *Rhizobium leguminosarum biovar trifolii* grown in soil with varying pH values and heavy metal concentrations. Agri Eco Environ 61:103–111

Jiang CY, Sheng XF, Qian M, Wang QY (2008) Isolation and characterization of a heavy metal-resistant *Burkholderia* sp. from heavy metal-contaminated paddy field soil and its potential in promoting plant growth and heavy metal accumulation in metal-polluted soil. Chemosphere 72(2):157–164

Kabata-Pendias A (2010) Trace Elements in Soils and Plants. CRC Press

Karthik C, Elangovan N, Kumar TS, Govindharaju S, Barathi S, Oves M, Arulselvi PI (2017) Characterization of multifarious plant growth promoting traits of rhizobacterial strain AR6 under Chromium (VI) stress. Microbiol Res 204:65–71

Kasowska D (2005) Flora of excavations and serpentine dumps of selected quarries and mines in Lower Silesia (in polish). Ann Silesiae 34: 105–113.

Kasowska D, Koszelnik-Leszek A (2014) Ecological features of spontaneous vascular flora of serpentine post-mining sites in Lower Silesia. Arch Environ Protect 40:33–52

Kazakou E, Dimitrakopoulos PG, Baker AJM, Reeves RD, Troumbis AY (2008) Hypotheses, mechanisms and trade-offs of tolerance and adaptation to serpentine soils: from species to ecosystem level. Biol Rev 83:495–508

Kieliszewski MJ, Lamport DT (1994) Extensin: repetitive motifs, functional sites, post-translational codes, and phylogeny. Plant J 5(2):157–172

Kierczak J, Neel C, Bril H, Puziewicz J (2007) Effect of mineralogy and pedoclimatic variations on Ni and Cr distribution in serpentine soils under temperate climate. Geoderma 142: 165–177

Kierczak J, Pędziwiatr A, Waroszewski J, Modelska M (2016) Mobility of Ni, Cr and Co in serpentine soils derived on various ultrabasic bedrocks under temperate climate. Geoderma 268:78–91

Koeuth T, Versalovic J, Lupski JR (1995) Differential subsequence conservation of interspersed repetitive *Streptococcus pneumoniae* BOX elements in diverse bacteria. Genome Res 5:408–418

Kruckeberg AR (2002) Geology and plant life: The effects of land forms and rock types on plants. University of Washington Press, Seattle, WA

Krzesłowska M (2011) The cell wall in plant cell response to trace metals: Polysaccharide remodeling and its role in defense strategy. Acta Physiol Plant 33(1):35–51

Kumar A, Maiti SK (2013) Availability of chromium, nickel and other associated heavy metals of ultramafic and serpentine soil/rock and in plants. Int J Emerging Technol Adv Eng 3: 256–268

Ladha JK, Reddy PM (2003) Nitrogen fixation in rice systems: state of knowledge and future prospects. Plant Soil 252:151–167

Lafuente A, Pajuelo E, Caviedes MA, Rodríguez-Llorente ID (2010) Reduced nodulation in alfalfa induced by arsenic correlates with altered expression of early nodulins. J Plant Physiol 167(4):286–291

Lafuente A, Perez-Palacios P, Doukkali B, Molina-Sanchez MD, Jimenez-Zurdo JI, Caviedes MA, Rodriguez-Llorente ID, Pajuelo E (2015) Unraveling the effect of arsenic on the model Medicago-Ensifer interaction: a transcriptomic meta-analysis. New Phytol 205:255–272

Lamport DTA, Kieliszewski MJ, Showalter AM (2006) Salt stress upregulates periplasmic arabinogalactan proteins: using salt stress to analyse AGP function. New Phytol 169:479–492

Le Gall H, Philippe F, Domon JM, Gillet F, Pelloux J, Rayon C (2015) Cell wall metabolism in response to abiotic stress. Plants 4:112–166

Li HF, Gray C, Mico C, Zhao FJ, McGrath SP (2009) Phytotoxicity and bioavailability of cobalt to plants in a range of soils. Chemosphere 75(7):979–986

Liu Y, Lam MC, Fang HHP (2001) Adsorption of heavy metals by EPS of activated sludge. Water Sci Technol 43:59–66

Lorite MJ, Estrella MJ, Escaray FJ, Sannazzaro A, Videira e Castro IM, Monza J, Sanjuán J, León-Barrios M (2018) The *Rhizobia-Lotus symbioses: deeply specific and widely diverse.* Front. Microbiol 9:2055.

Ma Y, Prasad MN, Rajkumar M, Freitas H (2011) Plant growth promoting rhizobacteria and endophytes accelerate phytoremediation of metalliferous soils. Biotechnol Adv 29(2):248–258

Markert B (1994) Plants as biomonitors - potential advantages and problems. In: Adriano DC, Chen ZS, Yang SS (eds) Biogeochemistry of trace elements. Science and Technology Letters, Northwood, NY, pp 601–613

Maynaud G, Brunel B, Mornico D, Durot M, Severac D, Dubois E, Navarro E, Cleyet-Marel J-C, Le Quéré A (2013) *Genome-wide transcriptional responses of two metal-tolerant symbiotic Mesorhizobium isolates to zinc and cadmium exposure*. BMC Genomics 14:292

Mengoni A, Schat H, Vangronsveld J (2010) Plants as extreme environments? Ni-resistant bacteria and Ni-hyperaccumulators of serpentine flora. Plant Soil 331:5–16

Mohamad R, Maynaud G, Le Quéré A, Vidal C, Klonowska A, Yashiro E, Cleyet-Marel J-C, Brunel B (2016) Ancient heavy metal contamination in soils as a driver of tolerant *Anthyllis vulneraria* rhizobial communities. Appl Environ Microbiol 83:e01735–e01716

Monza J, Fabiano E, Arias A (1992) Characterization of an indigenous population of rhizobia nodulating *Lotus corniculatus*. Soil Biol Biochem 24:241–247

Morales A, Alvear M, Valenzuela E, Castillo CE, Borie F (2011) Screening, evaluation and selection of phosphate-solubilising

fungi as potential biofertiliser. J Soil Sci Plant Nutr 11:89–103

Neubauer U, Nowack B, Furrer G, Schulin R (2000) Heavy metal sorption on clay minerals affected by the siderophore desferrioxamine B. Environ Sci Technol. 34(13):2749–2755

O'Lexy R, Kasai K, Clark N, Fujiwara T, Sozzani R, Gallagher KL (2018) Exposure to heavy metal stress triggers changes in plasmodesmatal permeability via deposition and breakdown of callose. J Exp Bot 69(15):3715–3728

Ogar A, Sobczyk Ł, Turnau K (2015) Effect of combined microbes on plant tolerance to Zn–Pb contaminations. Environ Sci Pollut Res 22:19142–19156

Pajuelo E, Rodríguez-Llorente ID, Lafuente A, Caviedes MA (2011) Legume–*Rhizobium* Symbioses as a Tool for Bioremediation of Heavy Metal Polluted Soils. In: Khan M, Zaidi A, Goel R, Musarrat J (eds) Biomanagement of Metal-Contaminated Soils. Environmental Pollution, vol 20. Springer, Dordrecht

Pal A, Wauters G, Paul AK (2007) Nickel tolerance and accumulation by bacteria from rhizosphere of nickel hyperaccumulators from serpentine soil of Andaman, India. Plant Soil 293(1-2):37–48

Parrota L, Guerriero G, Sergeant K, Cai G, Hausman J-F (2015) Target or barrier? The cell wall of early- and later- diverging plants vs cadmium toxicity: differences in the response mechanisms. Front. Plant Sci 6:133

Paunov M, Koleva L, Vassilev A, Vangronsveld GV (2018) Effects of different metals on photosynthesis: cadmium and zinc affect chlorophyll fluorescence in durum wheat. Int. J. Mol. Sci. 19(3):787

Pędziwiatr A (2018) Rock-type control of Ni, Cr, and Co phytoavailability in ultramafic soils. Plant Soil. 423:**339**–**362**

Pereira SIA, Lima AIG, Figueira EM, de Almeida PF (2006) Heavy metal toxicity in *Rhizobium leguminosarum* biovar *viciae* isolated from soils subjected to different sources of heavy-metal contamination: effects on protein expression. Appl Soil Ecol 33:286–293

Pikovskaya RI (1948) Mobilization of phosphorus in soil connection with the vital activity of some microbial species. Microbiology 17:362–370

Porter SS, Rice KJ (2013) *Trade-offs, spatial heterogeneity, and the maintenance of microbial diversity*. Evolution 67:599–608

Porter SS, Chang PL, Conow CA (2017) Association mapping reveals novel serpentine adaptation gene clusters in a population of symbiotic *Mesorhizobium*. ISME J. 11:248–262

Probst A, Liu H, Fanjul M, Liao B, Hollande E (2009) Response of *Vicia faba* L. to metal toxicity on mine tailing substrate: geochemical and morphological changes in leaf and root. Environ Exp Bot 66:297–308

Proctor JK (2003) Vegetation and soil and plant chemistry on ultramafic rocks in the tropical Far East. Perspect Plant Ecol Evol Syst 6(1):105–124

Purchase D, Miles RJ (2001) Survival and nodulating ability of indigenous and inoculated *Rhizobium leguminosarum* biovar *trifolii* in sterilized and unsterilized soil treated with sewage sludge. Curr Microbiol 42:59–64

Purchase D, Miles RJ, Young TWK (1997) Cadmium uptake and nitrogen fixing ability in heavy-metal-resistant laboratory and field strains of *Rhizobium leguminosarum* biovar *trifolii*. FEMS Microbiol Ecol 22:85–93

Rae AL, Perotto S, Knox JP, Kannenberg EL, Brewin NJ (1991) Expression of extracellular glycoproteins in the uninfected cells of developing pea nodule tissue. Molecular Plant-Microbe Interactions 4:563–570

Rai UN, Pandey K, Sinha S, Singh A, Saxena R, Gupta DK (2004) Revegetating fly ash landfills with Prosopis juliflora L.: impact of different amendments and Rhizobium inoculation. Environ Int 30:293–300

Rajkumar M, Prasad MNV, Freitas H, Ae N (2009) Biotechnological applications of serpentine soil bacteria for phytoremediation of trace metals. Crit Rev Biotechnol 29: 120–130

Raklami A, Oufdou K, Tahiri A-I, Mateos-Naranjo E, Navarro-Torre S, Rodríguez-Llorente ID, Meddich A, Redondo-Gómez S, Pajuelo E (2019) Safe cultivation of *Medicago sativa* in metal-polluted soils from semi-arid regions assisted by heat- and metallo-resistant PGPR. Microorganisms 7(7): 212. doi.org/10.3390/microorganisms7070212

Rathbun ER, Naldrett M, Brewin NJ (2002) Identification of a Family of Extensin-Like Glycoproteins in the Lumen of Rhizobium -Induced Infection Threads in Pea Root Nodules. Molecular Plant-Microbe Interactions 15(4):350–359

Reeves RD, Baker AJM, Becquer T, Echevarria G, Miranda ZJG (2007) The flora and biogeochemistry of the ultramafic soils of Goiás state, Brazil. Plant Soil 293:107–119

Rodríguez H, Fraga R (1999) Phosphate solubilizing bacteria and their role in plant growth promotion. Biotechnol Adv 17: 319–339

Rooney CP, Zhao FJ, McGrath SP (2007) Phytotoxicity of nickel in a range of European soils: influence of soil properties, Ni solubility and speciation. Environ Pollut 145(2):596–605

Rubio-Sanz L, Brito B, Palacios J (2018) Analysis of metal tolerance in *Rhizobium leguminosarum* strains isolated from an ultramafic soil. FEMS Microbiol Lett 365(4)

Salminen R, Batista MJ, Bidovec M, Demetriades A, De Vivo B, De Vos W, Duris M, Gilucis A, Gregorauskiene V, Halamic J, Heitzmann P, Lima A, Jordan G, Klaver G, Klein P, Lis J, Locutura J, Marsina K, Mazreku A, O'Connor PJ, Olsson SÅ, Ottesen R-T, Petersell V, Plant JA, Reeder S, Salpeteur I, Sandström H, Siewers U, Steenfelt A, Tarvainen T (2005) Geochemical Atlas of Europe. Part 1 –Background Information. Methodology and Maps. Geological Survey of Finland, Espoo, Finland, p 526

Šamaj J, Šamajova O, Peters M, Baluška F, Lichtscheidl I, Knox JP, Volkmann D (2000) Immmunolocalization of LM2 arabinogalactan protein epitope associated with endomembranes of plant cell. Protoplasma 212:186–196

Schmidt T, Schlegel HG (1994) Combined nickel-cobalt-cadmium resistance encoded by the ncc locus of *Alcaligenes xylosoxidans* 31A. J Bacteriol 176:7045–7054

Seregin I, Kozhevnikova A (2011) Histochemical methods for detection of heavy metals and strontium in the tissues of higher plants. Russ J Plant Physiol 58(4):721–727

Serpe MD, Nothnagel EA (1994) Effects of Yariv phenylglycosides on *Rosa* cell suspensions: Evidence for the involvement of arabinogalactan-proteins in cell proliferation. Planta 193:542

Sharma A, Jha AB, Dubey RS, Pessarakli M (2012) Reactive oxygen species, oxidative damage, and antioxidative defense

mechanism in plants under stressful conditions. J Bot. https://doi.org/10.1155/2012/217037

Sillanpää M (1982) Micronutrients and the nutrient status of soils: a global study. FAO, Soils Bulletin 48:1–444

Smith SE, Read DJ (1997) Mycorrhizal Symbiosis, 2nd edn. Academic Press, London

Star L, Matan O, Dardanelli MS, Kapulnik Y, Burdman S, Okon Y (2012) The *Vicia sativa* spp. nigra–*Rhizobium leguminosarum* bv. viciae symbiotic interaction is improved by *Azospirillum brasilense*. Plant Soil 356(1–2):165–174

Stearns JC, Shah S, Dixon DG, Greenberg BM, Glick BR (2005) Tolerance of transgenic canola expressing 1-aminocyclopropane-carboxylic acid deaminase to growth inhibition by nickel. Plant Physiol Biochem 43:701–708

Stępkowski T, Czaplińska M, Miedzinska K, Moulin L (2003) The variable part of the dnaK gene as an alternative marker for phylogenetic studies of rhizobia and related Alpha Proteobacteria. Syst Appl Microbiol 26:483–494

Stępkowski T, Moulin L, Krzyżańska A, McInnes A, Law IJ, Howieson J (2005) European origin of *Bradyrhizobium* populations infecting lupins and serradella in soils of Western Australia and South Africa. Appl Environ Microbiol 71: 7041–7052

Stępkowski T, Hughes CE, Law IJ, Markiewicz L, Gurda D, Chlebicka A, Moulin L (2007) Diversification of lupine Bradyrhizobium strains: evidence from nodulation gene trees. Appl Environ Microbiol 73:3254–3264

Sujkowska-Rybkowska M, Borucki W (2012) Structural changes in *Medicago truncatula* root nodules caused by short-term aluminum stress. Symbiosis 58(1-3):161–170

Sujkowska-Rybkowska M, Borucki W (2014) Accumulation and localization of extensin protein in apoplast of pea root nodule under aluminum stress. Micron. 67:10–19

Sujkowska-Rybkowska M, Borucki W (2015) Pectins esterification in the apoplast of aluminum-treated pea root nodules. J Plant Physiol 20;184:1-7.

Sujkowska-Rybkowska M, Ważny R (2018) Metal resistant rhizobia and ultrastructure of *Anthyllis vulneraria* nodules from zinc and lead contaminated tailing in Poland. Int J Phytorem 20(7):709–720

Sujkowska-Rybkowska M, Banasiewicz J, Rekosz-Burlaga H, Stępkowski T (2020) *Anthyllis vulneraria* and *Lotus corniculatus* on calamine heaps form nodules with *Bradyrhizobium liaoningense*-related strains harboring novel in Europe symbiotic *nifD* haplotypes. App Soil Ecol 151: 103539

Taghavi S, Garafola C, Monchy S, Newman L, Hoffman A, Weyens N (2009) Genome survey and characterization of endophytic bacteria exhibiting a beneficial effect on growth and development of poplar. Appl Environ Microbiol 75:748–757

Tsyganova AV, Seliverstova EV, Brewin NJ, Tsyganov VE (2019) Comparative analysis of remodelling of the plant–microbe interface in *Pisum sativum* and *Medicago truncatula* symbiotic nodules. Protoplasma doi.org/10.1007/s00709-019-01355-5

Vance CP, Johnson LEB, Stade S, Groat RG (1982) Birdsfoot trefoil (*Lotus corniculatus*) root nodules: morphogenesis and the effect of forage harvest on structure and function. Can J Bot. 60(4):505–518

Vanden Bosch KA, Bradley DJ, Knox JP, Perotto S, Butcher GW, Brewin NJ (1989) Common components of the infection thread matrix and the intercellular space identified by immunocytochemical analysis of pea nodules and uninfected roots. Europ Mol Biol Org J 8:335–342

Versalovic J, Schneider M, De Bruijn FJ, Lupski JR (1994) Genomic fingerprinting of bacteria using repetitive sequence-based polymerase chain reaction. In: Methods in Molecular and Cellular Biology. 5:25–40

Vessey JK (2003) Plant growth promoting rhizobacteria as biofertilizers. Plant Soil 255:571

Vincent JM (1970) A Manual for the Practical Study of Root Nodule Bacteria. Blackwell Scientific, Oxford

Wani PA, Khan MS (2013) Nickel detoxification and plant growth promotion by multi metal resistant plant growth promoting Rhizobium species RL9. Bull Environ Contam Toxicol 91(1)

Wani PA, Khan MS, Zaidi A (2007a) Effect of metal tolerant plant growth promoting *Bradyrhizobium* sp. (Vigna) on growth, symbiosis, seed yield and metal uptake by greengram plants. Chemosphere 70(1):36–45

Wani PA, Khan MS, Zaidi A (2008) Chromium reducing and plant growth promoting Mesorhizobium improves chickpea growth in chromium amended soil. Biotechnol Lett. 30:159–163

Yusuf M, Fariduddin Q, Hayat S, Ahmad A (2011) Nickel: an overview of uptake, essentiality and toxicity in plants. Bull Environ Contam Toxicol 86(1):1–17

Zahran HH (1999) Rhizobium legume symbiosis and nitrogen undersevere conditions in an arid climate. Microb Mol Biol Rev 63:968–989

Zaidi S, Usmani S, Singh BR, Musarrat J (2006) Significance of *Bacillus subtilis* strain SJ-101 as a bioinoculant for concurrent plant growth promotion and nickel accumulation in *Brassica juncea*. Chemosphere 64(6):991–997

Zhao CZ, Huang J, Gyaneshwar P, Zhao D (2017) *Rhizobium* sp. IRBG74 alters *Arabidopsis* root development by affecting auxin signaling. Front Microbiol 8: 2556.

Zielazinski EL, González-Guerrero M, Subramanian P, Stemmler TL, Arguello JM, Rosenzweig AC (2013) *Sinorhizobium meliloti* Nia is a P1B-5-ATPase expressed in the nodule during plant symbiosis and is involved in Ni and Fe transport. Metallomics 5(12):1614–1623

Żołnierz L (2007) Grass communities occurring in Lower Silesian serpentine - selected aspects of ecology. (in polish) Zesz. Nauk. UP we Wrocławiu, 555.

Zornoza P, Vázquez S, Esteban E, Fernández-Pascual M, Carpena R (2002) Cadmium-stress in nodulated white lupin: Strategies to avoid toxicity. Plant Physiol Biochem 40(12): 1003–1009